King's Research Portal

[Link to publication record in King's Research Portal](#)

Citation for published version (APA):
Claus, J., Patel, G., Autore, F., Colomba, A., Weitsman, G., Soliman, T. N., Roberts, S., Zanetti Domingues, L. C., Hirsch, M., Collu, F., George, R., Ortiz-Zapater, E., Barber, P. R., Vojnovic, B., Yarden, Y., Martin-Fernandez, M. L., Cameron, A., Fraternali, F., Ng, T., & Parker, P. J. (2018). Inhibitor-induced HER2-HER3 heterodimerisation promotes proliferation through a novel dimer interface. *eLife*, *7*, Article e32271. https://doi.org/10.7554/eLife.32271

1   Inhibitor-induced HER2-HER3 heterodimerisation promotes
2   proliferation through a novel dimer interface
3

4   **Authors**

5   Jeroen Claus[1]*, Gargi Patel[2,3]*, Flavia Autore[4], Audrey Colomba[1], Gregory Weitsman[2], Tanya

6   N. Soliman[1], Selene Roberts[5], Laura Zanetti-Domingues[5], Michael Hirsch[5], Francesca Collu[4],

7   Roger George[6], Elena Ortiz-Zapater[7], Paul Barber[4,12], Boris Vojnovic[4,8], Yosef Yarden[9], Marisa

8   Martin-Fernandez[5], Angus Cameron[1,10#], Franca Fraternali[4#], Tony Ng[2, 11,12#], Peter J.

9   Parker[1,13#]

10

11   **Affiliations**

12   1. Protein Phosphorylation Laboratory, The Francis Crick Institute, 1 Midland Road, London

13   NW1 1AT, UK

14   2. Richard Dimbleby Department of Cancer Research, Randall Division and Division of Cancer

15   Studies, Kings College London, Guy's Medical School Campus, London SE1 1UL, U.K.

16   3. Sussex Cancer Centre, Brighton and Sussex University Hospitals, Brighton BN2 5BE

17   4. Randall Division of Cell & Molecular Biophysics, Kings College London, Guy's Medical

18   School Campus, London SE1 1UL, U.K.

19   5. Central Laser Facility, Research Complex at Harwell, Science and Technology Facilities

20   Council, Rutherford Appleton Laboratory, Didcot, Oxford OX11 0QX, U.K.

21   6. The Structural Biology Science Technology Platform, The Francis Crick Institute, 1 Midland

22   Road, London NW1 1AT, UK

23   7. Department of Asthma, Allergy and Respiratory Science, King's College London, Guy's

24   Hospital, London, SE1 1UL, U.K.

25   8. Department of Oncology, Cancer Research UK and Medical Research Council Oxford

26   Institute for Radiation Oncology, Old Road Campus Research Building, Roosevelt Drive,

27   Oxford OX3 7DQ, U.K.

28   9. Department of Biological Regulation, Weizmann Institute of Science, Rehovot 76100,

29   Israel

30   10. Barts Cancer Institute, Queen Mary University of London, Charterhouse Square, London

31   EC1M 6BQ, U.K.

32   11. Breast Cancer Now Research Unit, Department of Research Oncology, Guy's Hospital

33   King's College London School of Medicine, London, SE1 9RT, U.K.

34   12. UCL Cancer Institute, 72 Huntley Street, University College London, London WC1E 6DD,

35   U.K.

36   13. School of Cancer and Pharmaceutical Sciences, King's College London, Guy's Campus,

37   London SE1 1UL, U.K.

38

39   ***** Authors contributed equally to this work

40   **#** Correspondence: a.cameron@qmul.ac.uk, franca.fraternali@kcl.ac.uk, tony.ng@kcl.ac.uk,

41   peter.parker@kcl.ac.uk

42

Abstract

44   While targeted therapy against HER2 is an effective first-line treatment in HER2^{+} breast

45   cancer, acquired resistance remains a clinical challenge. The pseudokinase HER3,

46   heterodimerisation partner of HER2, is widely implicated in the resistance to HER2-

47   mediated therapy. Here we show that lapatinib, an ATP-competitive inhibitor of HER2, is

48   able to induce proliferation cooperatively with the HER3 ligand neuregulin. This

49   counterintuitive synergy between inhibitor and growth factor depends on their ability to

50   promote atypical HER2-HER3 heterodimerisation. By stabilising a particular HER2

51   conformer, lapatinib drives HER2-HER3 kinase domain heterocomplex formation. This dimer

52   exists in a head-to-head orientation distinct from the canonical asymmetric active dimer.

53   The associated clustering observed for these dimers predisposes to neuregulin responses,

54   affording a proliferative outcome. Our findings provide mechanistic insights into the

55   liabilities involved in targeting kinases with ATP-competitive inhibitors and highlight the

56   complex role of protein conformation in acquired resistance.

57

Introduction

59   The epidermal growth factor receptor (EGFR) family of receptor tyrosine kinases plays a

60   major role in proliferative signalling in a variety of cancers (Baselga & Swain, 2009;

61   Yarden & Pines, 2012). Apart from EGFR (also known as ErbB1), the family consists of the

62   orphan receptor HER2 (ErbB2), the pseudokinase HER3 (ErbB3), and HER4 (ErbB4).

63 Overexpression of HER2 is an oncogenic driver in approximately 20% of all breast cancers

64 (Lovekin et al., 1991; Owens, Horten, & Da Silva, 2011; Slamon et al., 1987). The

65 high clinical relevance of these receptors has made them a target for directed therapy with

66 both antibodies and small molecule kinase inhibitors. In the case of HER2$^+$ breast cancer, the

67 monoclonal antibody trastuzumab (Herceptin) and its cytotoxic drug-conjugated derivative

68 trastuzumab-emtansine (Kadcyla), the monoclonal antibody blocking HER2-HER3

69 dimerisation pertuzumab (Perjeta), and the small molecule kinase inhibitor lapatinib

70 (Tykerb/Tyverb) have been successful in the clinic (Blackwell et al., 2010; D. Cameron et

71 al., 2017; Dieras et al., 2017; Geyer et al., 2006; Krop et al., 2017; Swain et al.,

72 2015; Verma et al., 2012).

73 While HER2 itself has no known ligand, HER3 binds the growth factor neuregulin

74 (NRG, also known as heregulin or HRG) to induce heterodimerisation and signalling

75 (Sliwkowski et al., 1994). HER3 has been implicated in therapeutic resistance to HER2-

76 targeted therapy through a variety of mechanisms, including receptor rephosphorylation,

77 HER3 overexpression and increased NRG production (reviewed in (Claus, Patel, Ng, &

78 Parker, 2014)). In terms of cellular signalling in response to HER-family kinase inhibition,

79 HER3-mediated buffering through the Akt/PKB signalling axis has been shown to be an

80 important factor in therapeutic resistance (Sergina et al., 2007).

81 The dimerisation of EGFR family members is a fluid process mediated by interaction

82 dynamics in practically every domain of the receptor. For EGFR, the ligand-bound, active

83 dimer shows an upright, back-to-back extracellular domain (ECD) interaction where both

84 receptors have bound ligand, although singly-bound dimers can also occur (Garrett et al.,

85 2002; P. Liu et al., 2012; Ogiso et al., 2002). Although HER2 has no known ligand, it

86 natively adopts this upright, dimerisation-ready ectodomain conformation (Garrett et al.,

87 2002). On the intracellular side, formation of the active kinase domain dimer is critically

88 affected by the conformation of the juxtamembrane domain (JMD (Jura, Endres, Engel,

89 Deindl, Das, Lamers, et al., 2009a; Thiel & Carpenter, 2007). The kinase domains

90 associate in an asymmetric dimer, which resembles the CDK/cyclin-like asymmetric dimer

91 interface (Jeffrey et al., 1995; X. Zhang, Gureasko, Shen, Cole, & Kuriyan, 2006). In

92 this canonical dimer one kinase (the "activator") allows the dimerisation partner (the

93 "receiver") to adopt an active conformation and become catalytically active. These various

94   conformations have also been observed in near-complete receptors using negative stain

95   electron microscopy (Mi et al., 2011). Of note in these receptor dimer formations was the

96   lack of active, asymmetrical kinase domain interactions when the receptor was bound to the

97   ATP-competitive inhibitor lapatinib (Mi et al., 2011). Although these interactions have

98   mainly been described in the context of EGFR homodimerisation, they remain a template

99   for the interactions of the rest of the EGFR family. The conformation of the active kinase

100   domain interaction has been validated for EGFR-HER3 and HER2-HER3 (Jura, Shan, Cao,

101   Shaw, & Kuriyan, 2009b; Littlefield et al., 2014; van Lengerich, Agnew, Puchner,

102   Huang, & Jura, 2017).

103   A multitude of studies, using a variety of techniques, have confirmed that EGFR-

104   family receptors can form higher order oligomers and that the exact nature of these

105   oligomers is modulated by a variety of conditions, including receptor density, ligand

106   presence, ligand type and temperature-dependent membrane behaviour (Clayton, 2005;

107   Clayton, Tavarnesi, & Johns, 2007; Y. Huang et al., 2016; Nagy, Claus, Jovin, &

108   Arndt-Jovin, 2010; Needham et al., 2016; Saffarian, Li, Elson, & Pike, 2008; van

109   Lengerich et al., 2017; Yang et al., 2007; R. Zhang et al., 2017).

110   Against the backdrop of such a multitude of association modes, it is clear that

111   conformational dynamics and structural rearrangements are an integral regulator of protein

112   behaviour in the EGFR family.

113

114   We have shown previously that within a kinase, in this case PKCε, occupation of the

115   nucleotide binding pocket with ATP (or an inhibitor) is a major determinant of protein

116   behaviour, conferring the structural stability required for protein-protein interactions to

117   occur and priming sites to be stably phosphorylated (A. J. M. Cameron, Escribano,

118   Saurin, Kostelecky, & Parker, 2009). Similar effects have been observed in several

119   additional kinases, including PKB/Akt, IRE1, and AMPK (Okuzumi et al., 2009; Papa,

120   Zhang, Shokat, & Walter, 2003; Ross et al., 2017; Wang et al., 2012).

121   A notable example of nucleotide binding pocket occupation inducing behaviour

122   independent of catalysis has been described for the RAF family, originally in cRAF, where the

123   inhibitor SB 203580 paradoxically induced activity (Eyers, Craxton, Morricel, Cohen, &

124   Goedert, 1998). More recently, a similar phenomenon has been shown in BRAF, where the

125   small molecule kinase inhibitor vemurafenib blocks the oncogenic mutant V600E, but

126   stabilises the wild type protein, promoting downstream proliferative signalling

127   (Hatzivassiliou et al., 2010; Mckay, Ritt, & Morrison, 2011; Poulikakos, Zhang,

128   Bollag, Shokat, & Rosen, 2010; Thevakumaran et al., 2014). Within the EGFR family,

129   we and others have shown previously that quinazoline inhibitors can cause homodimer

130   formation of EGFR, and EGFR-MET heterodimerisation, by stabilising particular kinase

131   domain conformers (Arteaga, Ramsey, Shawver, & Guyer, 1997; Bublil et al., 2010;

132   Lichtner, Menrad, Sommer, Klar, & Schneider, 2001; Ortiz-Zapater et al., 2017).

133

134   The structural, conformational role that nucleotide pocket occupation can fulfil is

135   particularly interesting in the context of pseudokinases, which have lost their catalytic

136   activity. Sequence analysis shows that many pseudokinases retain several of the conserved

137   residues involved in ATP-binding (Boudeau, Miranda-Saavedra, Barton, & Alessi, 2006;

138   Claus, Cameron, & Parker, 2013). And *in vitro* analysis of the pseudokinome showed that

139   many pseudokinases have nucleotide binding capability (Murphy et al., 2014).

140   In the case of these ATP-binding pseudokinases, where nucleotide binding does not

141   elicit phosphotransfer, the structural stability conferred by ATP binding may be integral to

142   protein function. This has been observed for the pseudokinase STRAD, which requires ATP

143   binding to sustain a heterotrimeric complex with LKB and MO25 (Zeqiraj, Filippi, Deak,

144   Alessi, & van Aalten, 2009a; Zeqiraj et al., 2009b). Similarly, in the pseudokinase

145   FAM20A ATP-binding, albeit in a non-canonical orientation, is essential for stabilising the

146   FAM20A/FAM20C complex (Cui et al., 2015; 2017). ATP binding is a structural

147   requirement for the JAK2 JH2 V617F mutant to promote pathogenic signalling (Hammarén

148   et al., 2015). In the pseudokinase MLKL, ATP-binding pocket occupation is essential for

149   membrane translocation and its role in necroptotic signalling (Hildebrand et al., 2014;

150   Murphy et al., 2013).

151   HER3 is able to bind ATP (crystallised as PDB ID 3XKK, 3LMG), as well as the Src/ABL

152   inhibitor Bosutinib (PDB ID 4OTW) (Boxer & Levinson, 2013; Davis et al., 2011; Jura,

153   Shan, Cao, Shaw, & Kuriyan, 2009b; Murphy et al., 2014; Shi, Telesco, Liu,

154   Radhakrishnan, & Lemmon, 2010). Considering the importance of HER3 as a

155   conformational partner in the HER2-HER3 heterodimer, and the established importance of

156 ATP-binding for complex formation in other pseudokinases, the role of nucleotide binding

157 pocket occupation in HER3 function warrants investigation.

158

159 Here we have integrated the study of kinase-autonomous conformational effects of

160 nucleotide binding pocket occupation with that of HER2-HER3 heterointeraction modalities

161 and downstream proliferative phenotypes in response to drug treatment. We show that

162 nucleotide pocket occupation in both HER2 and the pseudokinase HER3 is of great

163 conformational importance for kinase domain heterodimerisation and subsequent

164 proliferative signalling. In HER2$^+$ breast cancer cells this leads to an unexpected synergy

165 between the HER3 ligand NRG and the HER2 inhibitor lapatinib, by which their concomitant

166 binding promotes proliferation in 2D and 3D culture systems. Lapatinib is able to promote

167 heterodimerisation between the kinase domains of full-length HER2 and HER3 in cells.

168 However, this dimer interface is different from the canonical active EGFR-family dimer, and

169 it is necessary for the lapatinib/NRG combinatorial proliferative phenotype. Both the

170 lapatinib-induced heterodimer and the cooperative proliferation effects depend strongly on

171 the ability for the pseudokinase HER3 to bind ATP. Consistent with the model, occupying the

172 pseudokinase HER3 with the Src/Abl inhibitor bosutinib stabilises the pseudokinase domain

173 to the extent that it actually promotes HER2-HER3 heterodimerisation and downstream

174 proliferation.

175

176 **Results**

177

178 *Lapatinib-NRG co-treatment shows a synergistic effect on proliferation, dependent on HER3*

179 *ATP binding*

180 The sensitivity of a variety of oncogene-addicted cell lines to small molecule kinase

181 inhibitors can be counter-acted by the addition of growth factors (Wilson et al., 2012).

182 This includes the case of lapatinib-treated HER2$^+$ breast cancer cell lines, where NRG is seen

183 to mediate a rescue of drug toxicity (Novotny et al., 2016; Wilson et al., 2012). Using

184 different experimental procedures, we have investigated further these competing effects of

185 lapatinib and NRG on the proliferative behaviour of HER2$^+$ breast cancer cells.

186 　　　In SKBR3, BT474, AU565, and HCC1419 cells treated with a range of lapatinib

187 concentrations for 72 hours, the addition of 10 nM NRG rescues the drug-induced

188   cytotoxicity except at very high drug concentrations (Figure 1a, Figure 1-figure supplement

189   1a-c).

190   Interestingly, in the case of the SKBR3, BT474 and AU565 cell lines low

191   concentrations of lapatinib (~40-400 nM) are able to enhance proliferation in conjunction

192   with 10 nM NRG by 25%-30% compared to growth factor alone (Figure 1a, Figure 1-figure

193   supplement 1a-b). A partial response of this cooperative phenotype is observed in ZR75 and

194   HCC1419 cells (Figure 1-figure supplement 1c-d). This phenotype in SKBR3 cells, while

195   observed previously, has gone unremarked (Novotny et al., 2016; Wilson et al., 2012).

196   We corroborated our results with a cell counting assay, in which SKBR3 cells were treated

197   for 72 hours with 250 nM lapatinib or vehicle ± 10 nM NRG (Figure 1b). The emergent effect

198   of lapatinib plus NRG depends on lapatinib sensitivity. Two breast cancer cell lines with low

199   lapatinib sensitivity, MCF7 and HCC1569, show low inhibitor-growth factor cooperation

200   (Figure 1-figure supplement 1e-f). The growth phenotype in ZR75 may be partially explained

201   by its HER4 expression, considering that NRG is also a ligand for HER4 (Figure 1-figure

202   supplement 1g).

203   Although HER3 has been shown to bind lapatinib *in vitro* with very low affinity (Kd =

204   5.5 μM) (Davis et al., 2011), the synergistic behaviour between lapatinib and NRG occurs

205   in cells at a ~50x lower dose than the *in vitro* Kd, indicating that any binding of lapatinib to

206   HER3 would likely be minor under these conditions. Using a thermal shift assay (TSA), which

207   measures a shift in the thermal stability of a protein after ligand/inhibitor binding *in vitro*,

208   we also show that lapatinib does not strongly bind HER3 as compared to ATP and a panel of

209   other inhibitors (Figure 2a, see further below).

210   While EGF treatment rescued SKBR3 cells from the effects of low-concentration

211   lapatinib treatment, synergistic growth effects such as those observed with lapatinib-NRG

212   co-treatment were not observed for lapatinib-EGF co-treated SKBR3 or BT474 cells (Figure

213   1-figure supplement 1h-i). Although NRG is also a growth factor ligand for HER4, protein

214   levels of HER4 in SKBR3 cells are very low (Figure 1-figure supplement 1g). Additionally,

215   lapatinib is a strong inhibitor of both EGFR and HER4 (Davis et al., 2011). Taken together,

216   these data seem to exclude a significant role for EGFR and HER4 in the synergistic growth

217   observed for lapatinib-NRG co-treatment. Moreover, transient knockdown of HER3 with two

218   different siRNA oligonucleotides shows a modest, but consistent reduction in the

219   proliferative effect of ligand-inhibitor co-treatment, implicating HER3 as the relevant growth

220   factor-binding receptor for this NRG response (Figure 1-figure supplement 1j).

221   The proliferative effects of lapatinib and NRG on SKBR3 cells were also observed in

222   3D spheroid cultures. As seen in 2D culture systems, in 3D spheroid culture the addition of

223   NRG to lapatinib-treated cells rescues SKBR3 cells from lapatinib-induced

224   cytotoxicity/cytostasis (Figure 1c, Figure 1-figure supplement 1k-l). Lapatinib and NRG share

225   a cooperative effect on the induction of proliferation in 3D spheroid cultures, where

226   spheroid size is greater for inhibitor-ligand co-treatment conditions than for those treated

227   with growth factor alone.

228   The irreversible inhibitor neratinib binds the same inactive conformation as lapatinib

229   and with similar binding affinity (Davis et al., 2011). However, neratinib is an irreversible

230   inhibitor and forms a covalent bond with HER2^{C805}, a residue conserved in EGFR and HER4

231   but not HER3. Neratinib-NRG co-treatment did not show the synergistic proliferative

232   phenotype observed with lapatinib-NRG, in either a cell counting assay, or in 3D spheroid

233   formation (Figure 1-figure supplement 2a-d). Similarly, the induction of HER2 and HER3

234   phosphorylation seen in western blot analysis of lapatinib-NRG co-treated 3D spheroids was

235   absent in neratinib-NRG co-treatment (Figure 1-figure supplement 1l, Figure 1-figure

236   supplement 2d). This indicates that the proliferative phenotype observed for lapatinib is

237   likely to necessitate a dynamic, reversible inhibitor binding.

238   Collectively, the data from both 2D and 3D cultures show that there is a

239   counterintuitive synergy between the HER2 inhibitor lapatinib and the HER3 ligand NRG in

240   driving the proliferation of SKBR3 cells. This prompted us to examine the potential for novel

241   allosteric regulation of HER2-HER3 heterotypic interactions by both ligand and inhibitors.

242
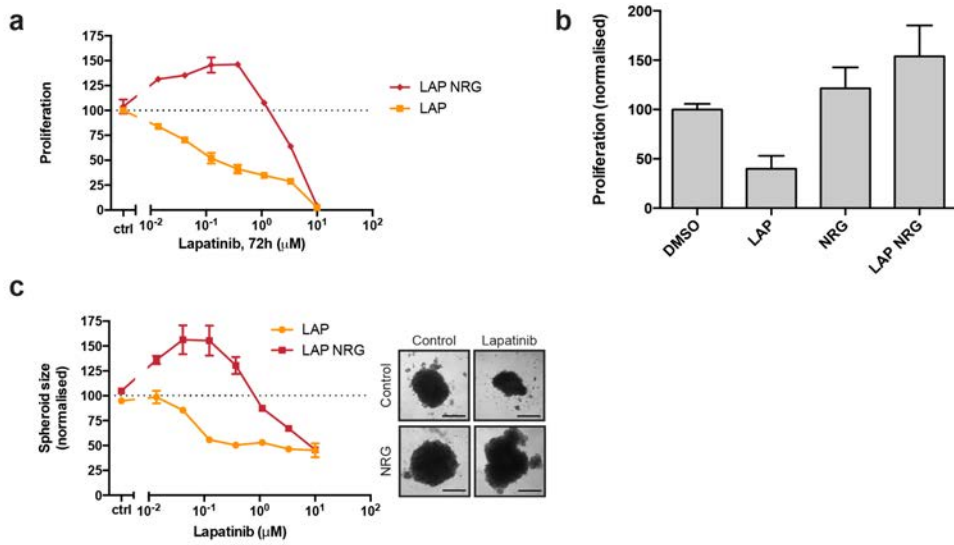
Figure 1

**Figure 1. Lapatinib and NRG have synergistic effects on SKBR3 growth in 2D and 3D culture systems**

(a) CellTiter-Glo® proliferation assay of SKBR3 cells after treatment for 72 hours with a range of lapatinib concentrations ± 10 nM NRG. **(b)** Cell counting assay of SKBR3 cells treated for 72 hours with DMSO or 250 nM lapatinib ± 10 nM NRG, before quantification of cell number on a Vi-CELL counter. **(c)** Quantification of SKBR3 3D spheroid area after 8 days of treatment with a range of lapatinib concentrations ± 10 nM NRG, with representative bright field micrographs. Scale bars 0.5 mm. All proliferation data represented as mean ± SEM of three independent experiments each performed in triplicate.

Corresponding data and statistics available as Figure 1 – Source Data 1.
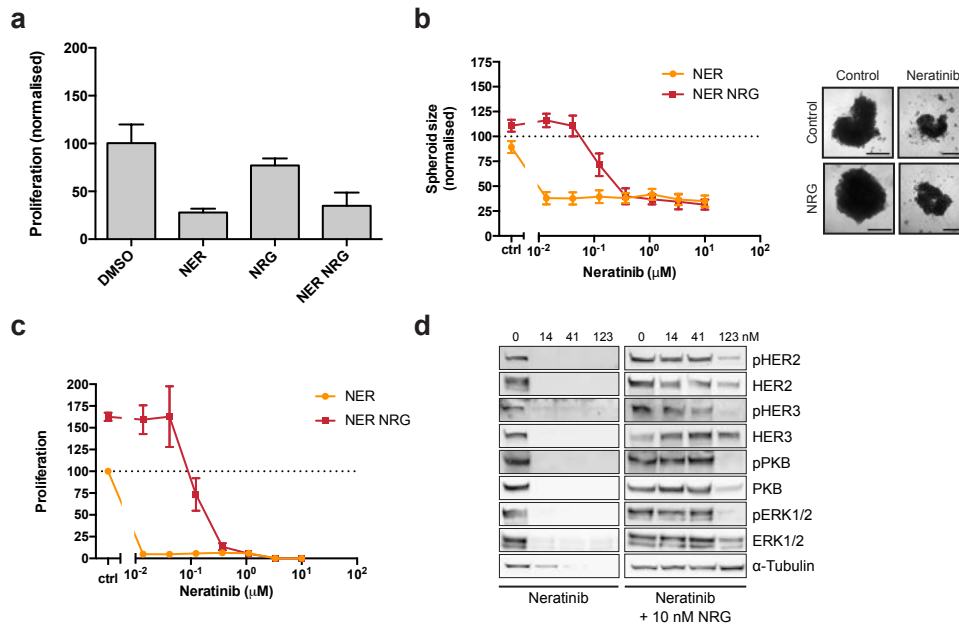
Figure 1-figure supplement 1

254
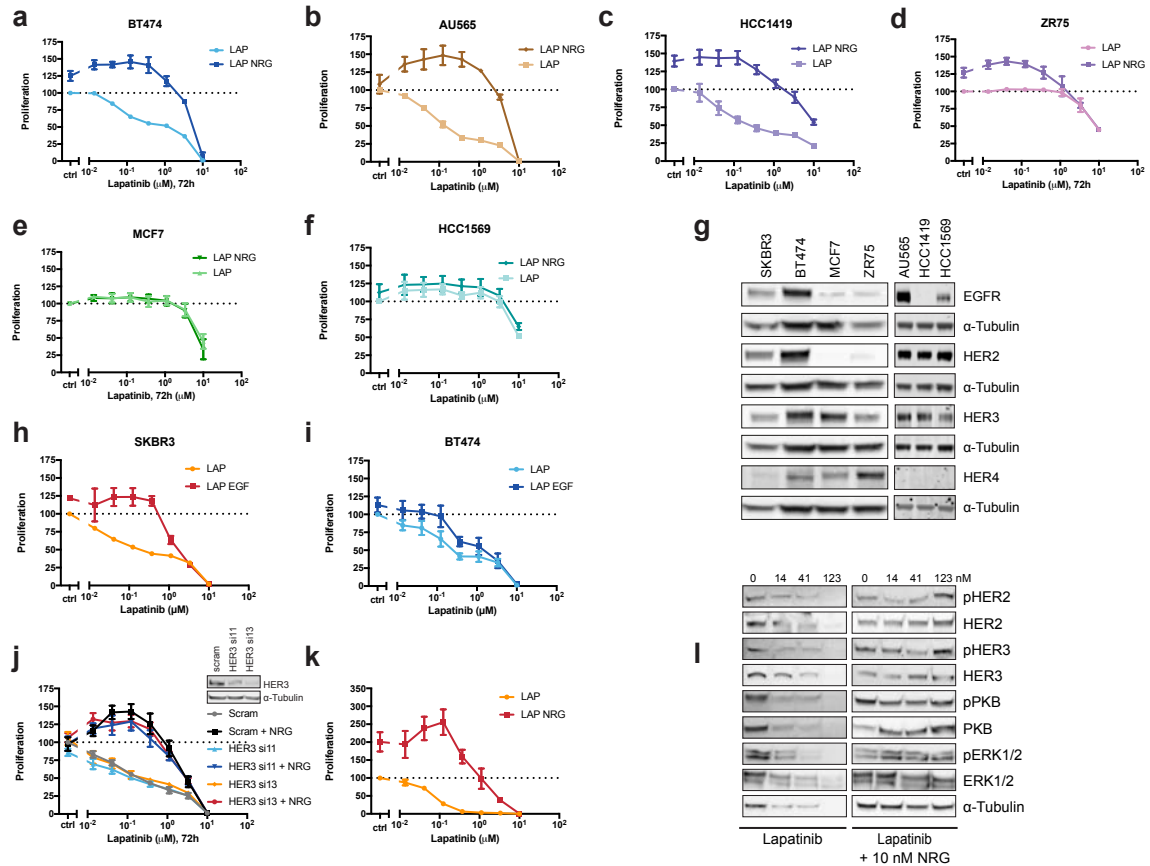
Figure 1-figure supplement 1. Effects of lapatinib and NRG on breast cancer cell proliferation

(a-f) BT474, AU565, HCC1419, ZR75, MCF7, and HCC1569 breast cancer cell lines were assayed for

proliferation in the response to lapatinib ± 10 nM NRG as described in Figure 1a. BT474 and AU565 represent

lapatinib-sensitive lines. HCC1419 and ZR75 represent partially-sensitive lines. MCF7 and HCC1569 represent

lapatinib-insensitive lines. **(g)** Western blot analysis of endogenous EGFR family protein levels in SKBR3, BT474,

AU565, HCC1419, ZR75, MCF7 and HCC1569 cell lines. **(h-i)** SKBR3 and BT474 cells were treated for 72 hours

with a titration of lapatinib ± 10 nM EGF, after which proliferation was measured using CellTiter-Glo®. **(j)**

CellTiter-Glo® proliferation assay of SKBR3 cells with transient siRNA knockdown of HER3 using single

oligonucleotides. Western blot denotes knockdown efficiency of HER3 si11 and HER3 si13 oligonucleotides. **(k)**

CellTiter-Glo® endpoint analysis of proliferation of SKBR3 spheroid cultures after 8 days of lapatinib ± NRG. **(l)**

Western blot analysis of SKBR3 spheroid cultures in conditions matched to Figure 1c/Figure 1-figure

supplement 1k. One representative example of three independent experiments is shown. All proliferation data

represented as mean ± SEM of three independent experiments each performed in triplicate, except for **(j)**,

which represents six independent experiments each performed in triplicate.

Corresponding data and statistics available as Figure 1-figure supplement 1 – Source Data 1.

270

10

Figure 1-figure supplement 2

271

Figure 1-figure supplement 2. The irreversible inhibitor neratinib does not show synergistic growth under ligand co-treatment conditions

(a) SKBR3 cells were treated for 72 hours with DMSO or 250 nM neratinib ± 10 nM NRG, before quantification of cell number on a Vi-CELL counter **(b)** Quantification of spheroid area after 8 days of treatment with a titration of neratinib. Representative bright field micrographs of SKBR3 cell 3D spheroids. Scale bars 0.5 mm. **(c)** CellTiter-Glo® endpoint analysis of spheroid cultures from **(b)**. **(d)** Western blot analysis of cell signalling in SKBR3 spheroids after 8 days of treatment. All proliferation data represented as mean ± SEM of three independent experiments each performed in triplicate. All Western blot shows a representative example of three independent experiments.

Corresponding data and statistics available as Figure 1-figure supplement 2 – Source Data 1.

284　*HER3 nucleotide pocket occupation is of structural importance*

285　To study the effects of ATP binding on HER3 function, we aimed to both stabilise and

286　destabilise the pseudokinase nucleotide-binding pocket. This would allow us to investigate

287　the importance of the structural role that nucleotide binding pocket occupation has been

288　shown to play in several (pseudo)kinases.

289　　　　To separate the structural and trace catalytic roles that ATP-binding could fulfill in

290　HER3, we used the ATP-competitive Src/Abl inhibitor bosutinib, which has been shown to

291　bind strongly to HER3 but not to other EGFR family members (Boxer & Levinson, 2013;

292　Davis et al., 2011). We compared bosutinib to a small panel of EGFR family inhibitors as

293　well as an additional Src inhibitor, dasatinib, in a thermal shift assay (TSA) (Figure 2a, Figure

294　2-figure supplement 1a). In line with previous observations, we confirmed that HER3

295　strongly binds bosutinib. Significantly, lapatinib was not able to provide a noticeable

296　thermal shift, which corresponds to previously published results indicating HER3 does not

297　bind lapatinib with high affinity (Davis et al., 2011). While lapatinib was able to confer

298　strongly increased thermal stability to HER2, bosutinib was not (Figure 2b). This is in line

299　with previously published data that indicates HER2 is not a strong bosutinib binder (Davis et

300　al., 2011).

301　　　　We hypothesised that bosutinib might be able to aid proliferation in a cellular

302　context by stabilising the nucleotide binding pocket of HER3 and helping sustain dimer

303　formation, analogous to vemurafenib-bound behaviour of BRAF. In a 2D proliferation assay,

304　SKBR3 cells treated with bosutinib over 72 hours show a dose dependent induction of

305　proliferation without additional NRG stimulation (Figure 2-figure supplement 1b). This

306　proliferative effect is sustained in eight-day treatments in 3D spheroid cultures (Figure 2c,

307　Figure 2-figure supplement 1d,e). The ability of bosutinib to induce SKBR3 cell proliferation

308　appears to be an EGFR-family mediated event, as lapatinib treatment can curtail its effects

309　in a dose-dependent manner (Figure 2-figure supplement 1e).

310

311　In order to destabilise the HER3 nucleotide binding pocket we made the triple mutant

312　HER3^{KGG}. HER3^{K742} was mutated to methionine to hinder ATP α-phosphate coordination,

313　which by itself has been shown to reduce HER3 mant-ATP binding affinity (Shi et al., 2010).

314　To obstruct ATP binding further, double aspartates were introduced in the glycine-rich loop

315　(HER3$^{G716D/G718D}$) to mimic the pseudokinase-specific aspartate residue observed in the

316   glycine-rich loop of VRK3 (Scheeff, Eswaran, Bunkoczi, Knapp, & Manning, 2009),

317   adding a negative charge in the area where the ATP phosphates would normally sit.

318   Introduction of this ATP-binding deficient HER3^{KGG} mutant into MCF7 cells shows abrogation

319   of ligand-induced trans-phosphorylation of HER3 by HER2 (Figure 2d). SKBR3 cells

320   ectopically expressing HER3^{wt} or HER3^{KGG} show a differential proliferative behaviour upon

321   lapatinib ± NRG treatment. This indicates a critical role for HER3 ATP binding in order to

322   sustain inhibitor-growth factor cooperative proliferation (Figure 2-figure supplement 1f).

323   The bosutinib binding of HER3^{wt}, HER3^{KGG}, and the proposed drug de-sensitised

324   HER3^{T787M} (Boxer & Levinson, 2013; Dong, Guo, & Xue, 2017), was investigated using an in-

325   cell thermal shift assay (CETSA)(Jafari et al., 2014; Reinhard et al., 2015). Where wild type

326   HER3 showed increased thermal stability in cells in the presence of 50 nM bosutinib,

327   HER3^{KGG} did not (Figure 2-figure supplement 1g). Ectopic expression of wild type HER3, but

328   not HER3^{KGG} or HER3^{T787M}, enhances bosutinib-mediated proliferation, indicating this

329   behaviour is driven by bosutinib binding to HER3 directly (Figure 2e). Both HER3^{KGG} and

330   HER3^{T787M} showed normal localization to the plasma membrane, as measured by flow

331   cytometry, indicating that these mutations did not compromise the receptor and its traffic

332   to the plasma membrane (Figure 2-figure supplement 2).

333   The HER3^{KGG} and bosutinib results indicate that nucleotide pocket occupation in

334   HER3 is essential for its ability to sustain a proliferative signalling pathway under distinct

335   circumstances: in the acute response to growth factor, in promoting ligand-inhibitor

336   cooperative proliferation and even after treatment with a HER3-binding inhibitor. This

337   indicates a critical structural role for HER3 ATP-binding pocket occupation in its ability to

338   sustain heterointeractions and proliferation. Considering the proliferative effects observed

339   with the HER3-binding inhibitor bosutinib, our results also suggest that any residual

340   transferase activity HER3 retains does not appear to be important in these responses *in vivo*

341   unless we invoke a hit-and-run mechanism of action for bosutinib on HER3 which would

342   seem unlikely.

343

Figure 2
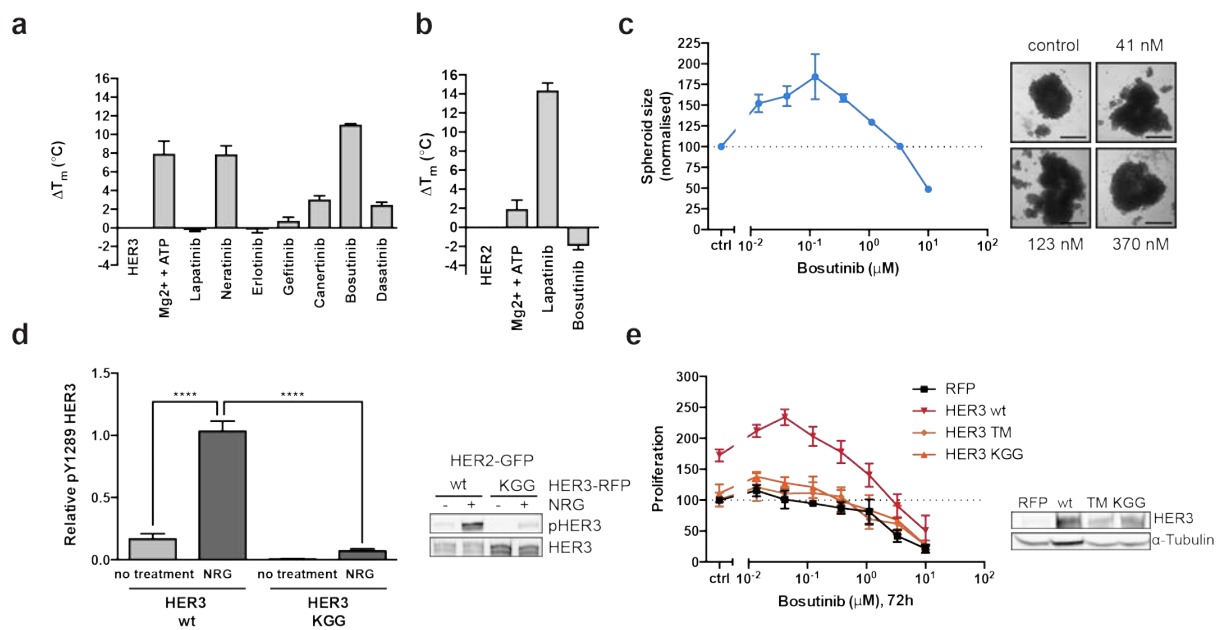
344

345 **Figure 2 HER3 ATP-binding pocket occupation is necessary and sufficient to drive SKBR3 cell growth**

346 **(a)** In vitro TSA binding assay of HER3 with selected kinase inhibitors. **(b)** In vitro TSA binding assay of HER2

347 with lapatinib and bosutinib. **(c)** Quantification of spheroid size after eight days of treatment with a titration of

348 bosutinib with representative bright field micrographs of SKBR3 cell spheroids after eight days of bosutinib

349 treatment. Scale bars signify 0.5 mm. **(d)** Transient co-transfection of MCF7 cells with HER2^{wt}-GFP and HER3^{wt}-

350 RFP or HER3^{KGG}-RFP. Cells were serum starved for one hour, followed by 10nM NRG or vehicle for ten minutes.

351 HER3 phosphorylation on Y1289 was measured by Western blot and analysed by densitometry relative to total

352 HER3. **(e)** SKBR3 cells were transfected with RFP empty vector, HER3^{wt}-RFP, HER3^{T787M}-RFP or HER3^{KGG}-RFP. 72

353 hours of bosutinib treatment was initiated 24 hours post-transfection. Proliferation was measured using

354 CellTiter-Glo®.

355 TSA data represented as mean ± SEM of (a) two independent experiments each performed quadruplicate, or

356 (b) three independent experiments each performed in at least quadruplicate. Proliferation data represented as

357 mean ± SEM of three independent experiments each performed in at least triplicate. Western blot data shown

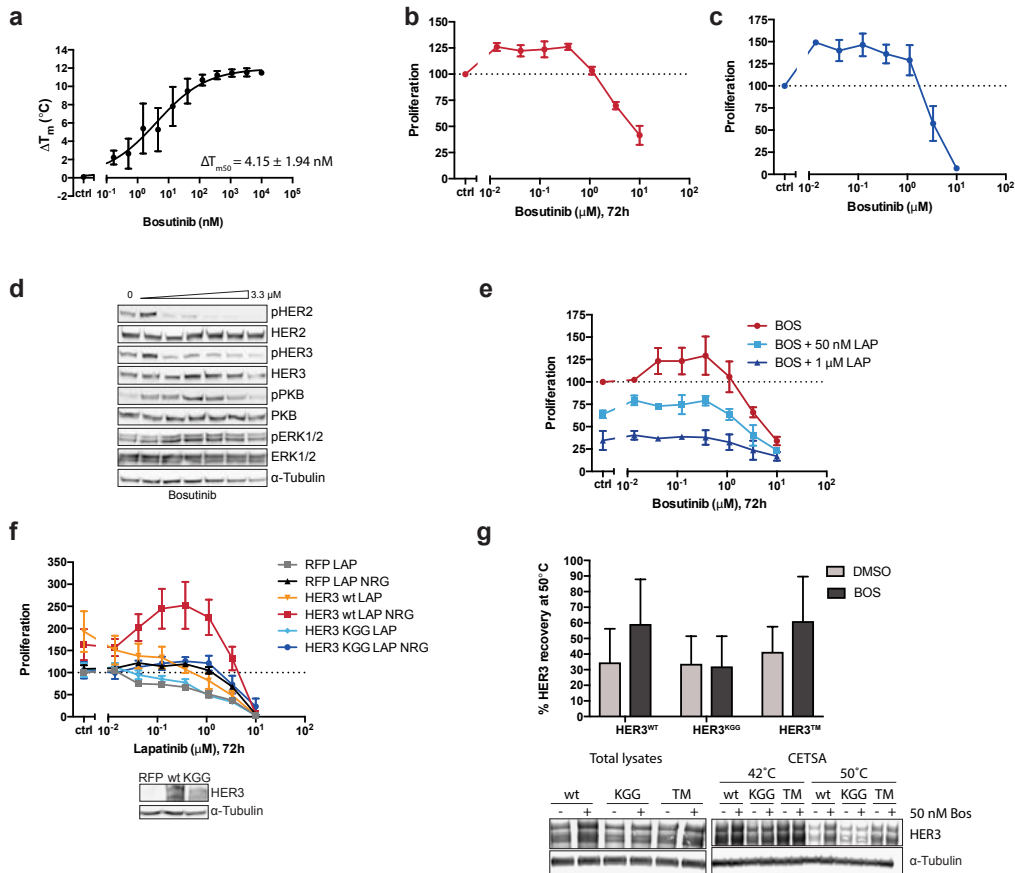358 as mean ± SD for three independent experiments. Western blot quantifications analysed by one-way ANOVA.

359 ****, p≤0.0001

360 Corresponding data and statistics available as Figure 2 – Source Data 1.

361

362

Figure 2-figure supplement 1

Figure 2-figure supplement 1. The effects of HER3 ATP-binding pocket occupation on drug-induced cell proliferation.

(a) TSA of HER3 kinase domain and a titration of bosutinib shows a ΔT_{m50} of 4.15 ± 1.94 nM.

(b) SKBR3 cells were treated with a range of bosutinib concentrations for 72 hours and proliferation was measured using CellTiter-Glo® **(c)** CellTiter-Glo® endpoint quantification of spheroid cultures from Figure 2b.

(d) Western blot analysis of spheroid cultures treated as in **(c)**. **(e)** 2D proliferation of SKBR3 cells using a titration of bosutinib ± lapatinib (50 nM or 1 µM) for 72 hours. **(f)** SKBR3 cells were transiently transfected with vector-RFP, HER3^{wt}-RFP, or HER3^{KGG}-RFP and treated with lapatinib ± 10 nM NRG for 72 hours. **(g)** CETSA analysis of bosutinib binding to HER3^{wt}, HER3^{KGG}, or HER3^{T787M}. Lysates of COS7 cells ectopically expressing HER3-RFP were treated with DMSO or 50 nM bosutinib, after which samples were split and matching samples incubated at either 42°C or 50°C. Western blot analysis shows HER3 recovery at 50°C compared to 42°C. Data in (a-f) presented as mean ± SEM of three independent experiments each performed in triplicate. Weste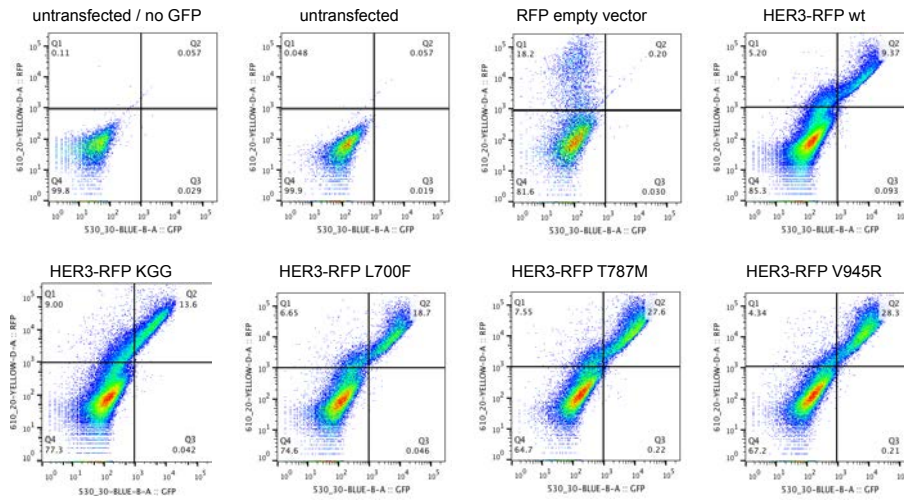rn blot data in (d) shows a representative example of three independent experiments. Data in (g) presented as mean ± SD of four independent experiments. Corresponding data and statistics available as Figure 2-figure supplement 1 – Source Data 1.

Figure 2-figure supplement 2

380

Figure 2-figure supplement 2. Cell surface expression of HER3 mutants.

Flow cytometric analysis of membrane localisation of all HER3-RFP constructs used in this study. Live SKBR3 cells were stained with GFP-conjugated anti-HER3 to show the combination of transfected and endogenous HER3 on the membrane. All HER3-RFP constructs show membrane localisation, as represented by the top right quadrants. Representative flow cytometry plots from one of two independent experiments.

388   *Lapatinib binding induces HER2-HER3 heterodimerisation*

389   The stability conferred to a protein kinase by small molecule inhibitor binding has been

390   shown to play an important role in the promotion of protein-protein interactions. We

391   investigated the potential role of lapatinib to similarly promote HER2-HER3

392   heterodimerisation by stabilising particular protein conformations in HER2 using a FRET-

393   FLIM approach. We measured drug-induced heterodimerisation of HER2 and HER3, as we

394   have done previously in the case of drug-induced dimerisation of the EGF receptor (Bublil

395   et al., 2010; Coban et al., 2015).

396   At endogenous protein levels in SKBR3 cells, we observe lapatinib-driven HER2-HER3

397   heterodimerisation to levels similar to those seen with NRG (Figure 3a). Interestingly, the

398   lapatinib-induced dimerisation occurs in the absence of exogenously added NRG, indicating

399   a HER2-HER3 dimer that is driven primarily through intracellular domain interactions. MCF7

400   cells, which express low levels of endogenous HER2 and HER3 compared to SKBR3, also

401   display lapatinib-induced heterodimerisation of ectopically expressed GFP-HER2^{wt} and HA-

402   HER3^{wt} (Figure 3b).

403   As discussed above, occupation of the nucleotide binding pocket in HER3 is of

404   importance for its ability to sustain proliferation. This is also reflected in the case of

405   lapatinib-induced heterodimer formation, where the introduction of the nucleotide pocket

406   compromised HER3^{KGG} mutant strongly disrupts inhibitor-promoted heterodimerisation

407   (Figure 3c). In line with the proliferative effects described above, bosutinib was also able to

408   directly promote heterodimerisation between HER2 and HER3 (Figure 3d).

409   Using stochastic optical reconstruction microscopy (STORM), we analysed receptor

410   clustering in SKBR3 cells. Treatment with either NRG, lapatinib, or bosutinib showed a shift

411   in cluster population size compared to control, implying the formation of higher-order

412   oligomers rather than dimers (Figure 3e,f). The exact HER2-HER3 stoichiometry in these

413   drug-treated oligomers remains elusive, because these experimental conditions allowed us

414   to count only cluster size for either HER2 or HER3, not both at the same time. Therefore, it is

415   expected that the observed HER3 clusters also contain uncounted HER2 receptors, and vice

416   versa, as evident in the FRET-FLIM data.

417

418

Figure 3
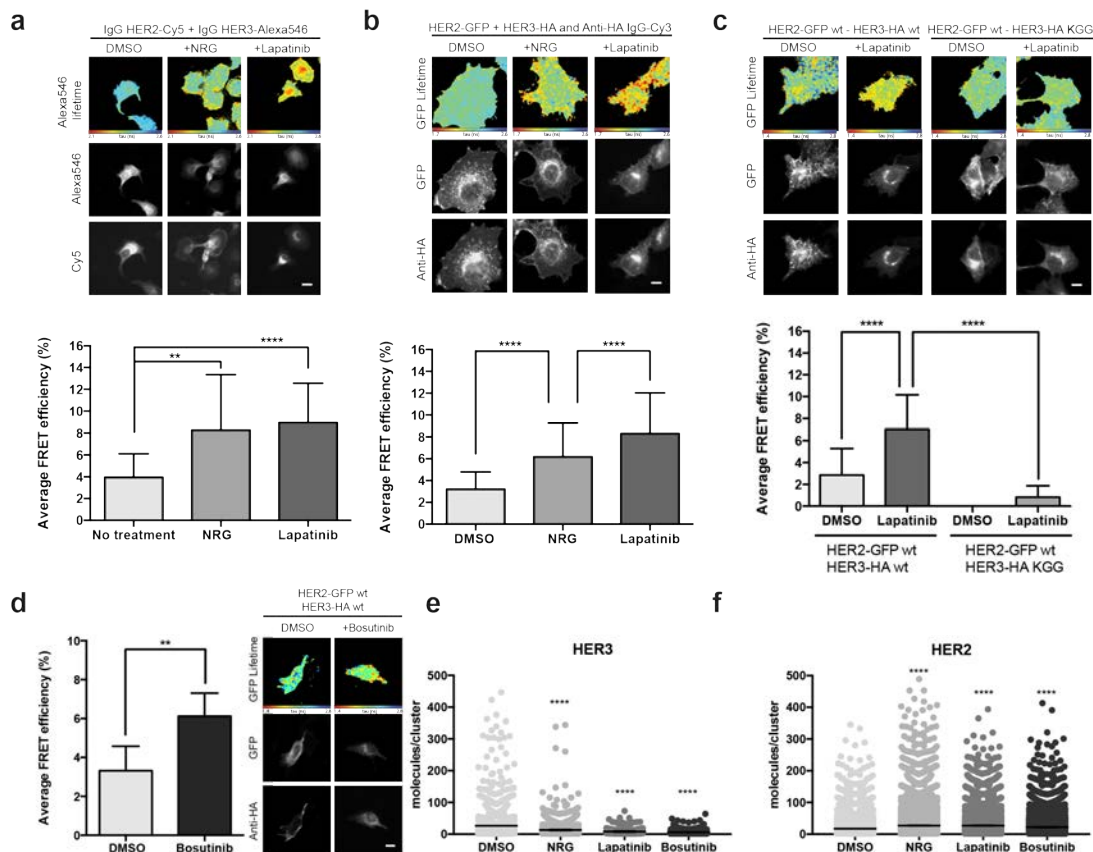
Figure 3 Inhibitor-induced HER2-HER3 heterotypic interactions

(a) FRET-FLIM analysis of endogenous HER2-HER3 association in SKBR3 cells, serum starved for 1 hour, and stimulated with 6.7 nM NRG for 15 minutes, or inhibited with lapatinib (10μM) for 1 hour, prior to fixation and staining with IgG α-HER2-Cy5 and IgG α-HER3-Alexa546 overnight, at 4ºC. **(b)** MCF7 cells were transfected with vectors encoding HER2^{wt}-GFP and HER3^{wt}-HA. Cells were incubated as in **(a)** and stained with anti-HA antibody conjugated to Alexa-546 (controls treated with vehicle). **(c)** MCF7 cells were transfected with vectors encoding HER2^{wt}-GFP and HER3^{wt}-HA or HER3^{KGG}-HA. Cells treated with lapatinib (10μM) for 1 hour, prior to fixation and staining with anti-HA antibody conjugated to Alexa-546. **(d)** SKBR3 cells were treated with bosutinib (50 nM, 1 hour), and stained as in **(b)**. **(e)(f)** Molecules/cluster measurements from STORM data taken of SKBR3 cells labelled with HER2Affibody-Alexa488 and HER3Affibody-Alexa647 or NRG-Alexa647 ± 14 nM lapatinib or 41 nM bosutinib.

Cumulative FRET-FLIM histograms show average FRET efficiency from three independent experiments. **, p≤0.01; **** p≤0.0001 Scale bars 5 μm. Clustering data represents mean combination of two independent experiments with each measuring >1000 clusters. Clustering data presented as mean with 95% CI. Corresponding data and statistics available as Figure 3 – Source Data 1.

Disruption of the active HER2-HER3 interface

437 The active signalling dimer in the EGFR family adopts an asymmetric orientation, in which

438 there is a distinct division of labour in the activator-receiver pairing. One kinase (the

439 activator kinase) does not phosphorylate substrates, but binds in a way that helps its

440 heterodimerisation partner (the receiver kinase) in adopting an active conformation. The

441 receiver kinase is then capable of substrate phosphorylation. Originally described for EGFR

442 homodimerisation, and similar to the Cyclin/CDK binding mode (Jeffrey et al., 1995; X.

443 Zhang et al., 2006), this canonical active dimerisation interface has been reported across

444 the EGFR family including the heterodimerisation of HER3, which can only perform the

445 activator role (Jura, Shan, Cao, Shaw, & Kuriyan, 2009b; Littlefield et al., 2014; van

446 Lengerich et al., 2017). Mutations that disrupt this active interface in both the activator

447 and receiver partner kinases are well-documented and are schematically highlighted (Figure

448 4a, Figure 4-video 1).

449 In the case of the active, activator/receiver interface, HER3 buttresses the inward

450 orientation of the HER2 α-C helix, leaving no space for the HER2 α-C helix to adopt the "out"

451 orientation characteristic of the inactive conformation. We modelled the potential effects of

452 HER2 α-C helix positioning on lapatinib binding to test whether canonical activator/receiver

453 orientation (in which the HER2 α-C helix is pushed inwards) would give sufficient space to

454 still accommodate lapatinib. Our modelling showed that, for a HER2 α-C helix in the active,

455 "in" position, lapatinib binding results in a potential steric clash with HER2^{E770}/HER3^{M774}

456 (Figure 4-figure supplement 1a,b). A general decrease of the nucleotide binding pocket

457 volume from 756 Å^3 to 232 Å^3 (calculated using SURFNET v1.5(Laskowski, 1995)) supports

458 these predictions.

459 To further test whether the lapatinib-induced HER2-HER3 is adopting the canonical

460 activator/receiver orientation, we used FRET-FLIM to investigate lapatinib-induced dimer

461 formation. The I714Q mutation in HER2, which renders the receptor receiver-impaired,

462 disrupted the lapatinib-driven HER2-HER3 association, indicating it is retained in the

463 lapatinib-induced dimer interface (Figure 4b). However, the reciprocal activator-impaired

464 mutation in HER3 (HER3^{V945R}) did not disrupt lapatinib-mediated heterodimerisation,

465 although it efficiently suppressed the canonical active dimer after ligand-induced

466 heterodimerisation (Figure 4c).

467   It is surmised that the inhibitor binding is able to robustly induce a heterodimer

468   between HER2 and HER3, which is distinct from the canonical active heterodimer induced

469   after growth factor stimulation. The orientation of this non-canonical lapatinib-driven

470   heterodimer retains HER2^{I714} in the dimer interface, giving us a starting point for *in silico*

471   molecular modelling to investigate potential dimer conformations distinct from the well-

472   described active dimer.

473

474
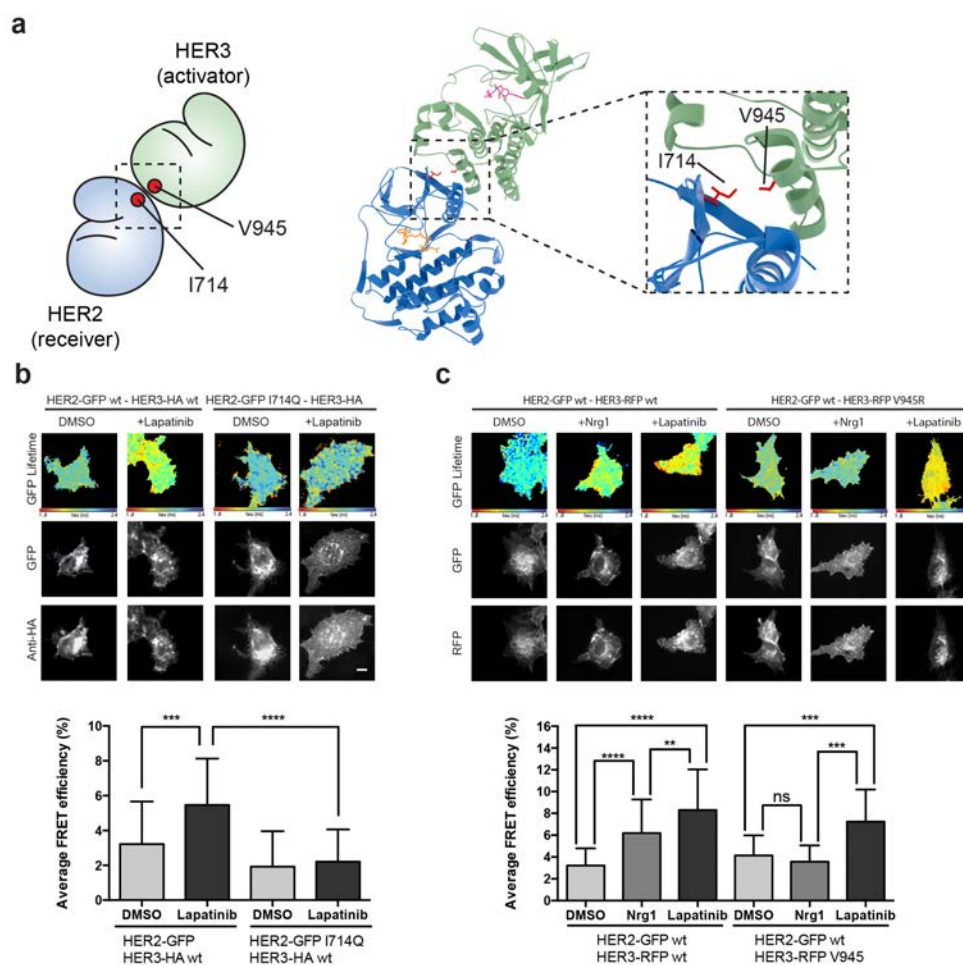
Figure 4 The lapatinib-induced HER2-HER3 dimer is distinct from the active, asymmetric HER2-HER3 dimer orientation

(a) Schematic representation and molecular model of HER2-HER3 active, asymmetric kinase domain dimer orientation. Insert denotes interaction interface. **(b)** MCF7 cells were transfected with vectors encoding HER2^{wt}-GFP or HER2^{I714Q}-GFP and HER3^{wt}-HA. Cells were treated as described in Figure 3 and HER2-HER3 association was measured by FRET-FLIM. **(c)** MCF7 cells were transfected with vectors encoding HER2-GFP and HER3^{wt}-RFP or HER3^{V945R}-RFP. Cells were incubated as described above, and treated with DMSO, lapatinib or NRG prior to fixation. Data represents mean ± SEM. *, p ≤0.05; **, p≤0.01, ***, p≤0.001; ****, p≤0.0001 by One-way ANOVA. Scale bars 5 µm
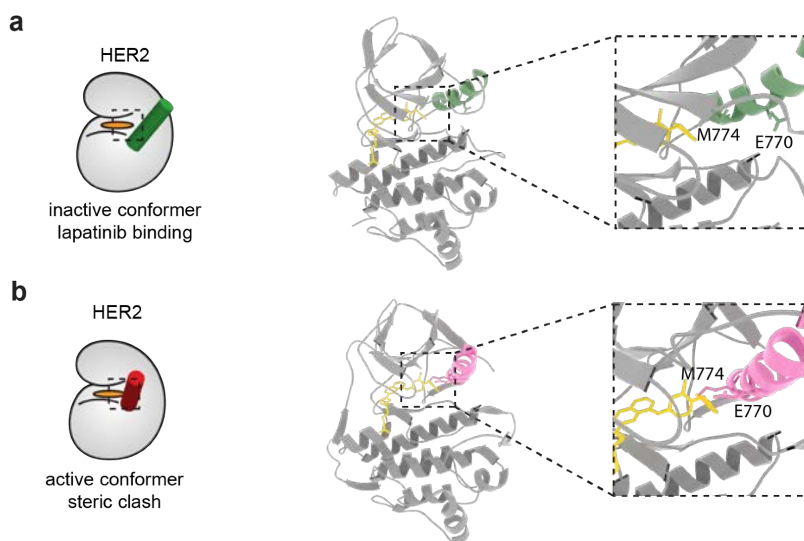
Corresponding data and statistics available as Figure 4 – Source Data 1. Molecular model for the interaction in **(a)** available as Figure 4 – Source Data 2.

Figure 4-video 1

Interface view of the molecular model of an active HER2-HER3 heterodimer, with HER2^{I714} and HER3^{V945} highlighted.

Figure 4-figure supplement 1

491

492 **Figure 4-figure supplement 1. Model of lapatinib binding in HER2 inactive and active conformations shows a**

493 **potential steric clash.**

494 **(a)** Lapatinib docking in HER2, with the HER2 active site displayed in the inset. Lapatinib binds the inactive

495 conformation of HER2 where the α-C helix is in the "out" position. E770 and M774 on the HER2 α-C helix

496 highlighted. **(b)** Lapatinib docked into the active conformation of HER2. The α-C helix is in the "in" position,

497 causing a steric clash between E770/M774 and lapatinib.

498 Molecular models for inhibitor docking in **(a)** and **(b)** available as Figure 4-figure supplement 1 – Source Data 1

499 and 2.

500

501

502 *Lapatinib drives a novel HER2-HER3 heterodimerisation interface*

503 In the case of type II kinase inhibitors such as lapatinib, the inhibitor stabilises an inactive

504 conformation of the kinase domain, where the α-C helix is tilted outwards. As HER3 lacks

505 the conserved glutamate residue in the α-C helix, HER3^{K742} is unable to form the salt bridge

506 normally observed in active kinase domain structures (Huse & Kuriyan, 2002). The HER3

507 ATP-bound conformation therefore does not show a classical active conformation with the

508 α-C helix tilted inward (Jura, Shan, Cao, Shaw, & Kuriyan, 2009b; Shi et al., 2010) ,

509 but instead resembles the inactive conformation seen in kinases bound to type II inhibitors

510 such as lapatinib. Because lapatinib-bound HER2 and ATP-bound HER3 adopt similar

511 conformations, there is a possibility that the lapatinib-induced, inactive dimer is oriented

512 symmetrically.

513 　　In the crystal lattices of EGFR and HER3 kinase domains, two different symmetrical

514 interaction interfaces have been observed (Jura, Endres, Engel, Deindl, Das, Lamers, et

515 al., 2009a; Jura, Shan, Cao, Shaw, & Kuriyan, 2009b). We used molecular modelling to

516 investigate the potential for HER3 and lapatinib-bound HER2 to adopt either of these

517 conformers (Figure 5a-b, Figure 5-figure supplement 1a-b). HER2^{I714} is present in the

518 interaction interface of both the EGFR-like, staggered orientation, as well as in the head-to-

519 head, HER3-like orientation. This falls in line with the FRET-FLIM data in Figure 4 that

520 suggests the retained presence of the HER2^{I714} residue in the lapatinib-induced dimer

521 interface.

522 　　On the basis of these models, we designed pairs of mutations in HER2 that would

523 exclusively disrupt one of the potential heterodimer orientations (Figure 5-figure

524 supplement 1, Figure 5-video 1-2). For the EGFR-like, staggered dimer we substituted two

525 hydrophobic residues on HER2 with two positively charged residues, HER2$^{I748R/V750R}$, which

526 should lead to repulsion from the positively charged residues, K998 and K999, lying on the

527 HER3 side of the interface.

528 　　Likewise, for the HER3-like, head-to-head dimer we predicted that the

529 HER2$^{N764R/K765F}$ mutant would disrupt the dimerisation interface. The substitution of an

530 asparagine residue (HER2^{N764}) with a positively charged arginine should lead to repulsion

531 from a positively charged HER3 residue (HER3^{R702}), lying within a radius of 4Å and opposite

532 to HER2^{N764}, therefore causing severe disruption of the HER3-like dimer interface.

533   Furthermore, the substitution of a lysine residue (HER2^{K765}) with a bulky, hydrophobic

534   residue such as phenylalanine should generate clashes at this HER2-HER3 interface.

535   These dimer interface mutants were introduced into our FRET-FLIM assay for

536   investigation of the lapatinib-induced heterodimerisation conformer (Figure 5c). The

537   HER2$^{N764R/K765F}$ mutant disrupted heterodimerisation upon lapatinib binding, whereas

538   HER2$^{I748R/V750R}$ showed no difference in heterodimer formation.
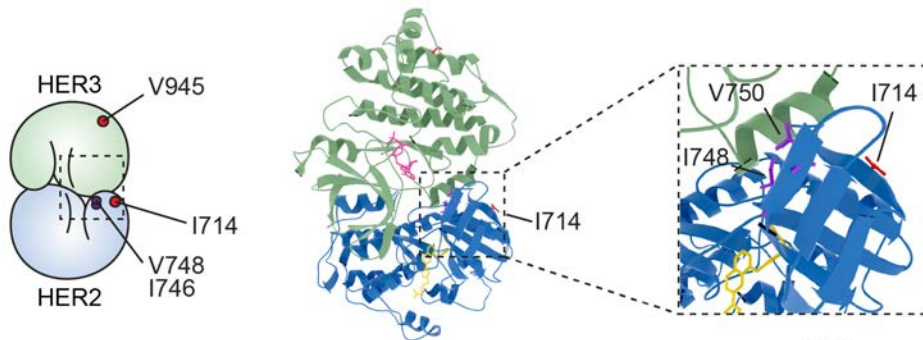
539   This mutational FRET/FLIM data is consistent with our model that the lapatinib-

540   induced HER2-HER3 heterodimer adopts a symmetrical, head-to-head orientation, similar to

541   the one observed in the HER3 kinase domain crystal lattice (Jura, Shan, Cao, Shaw, &

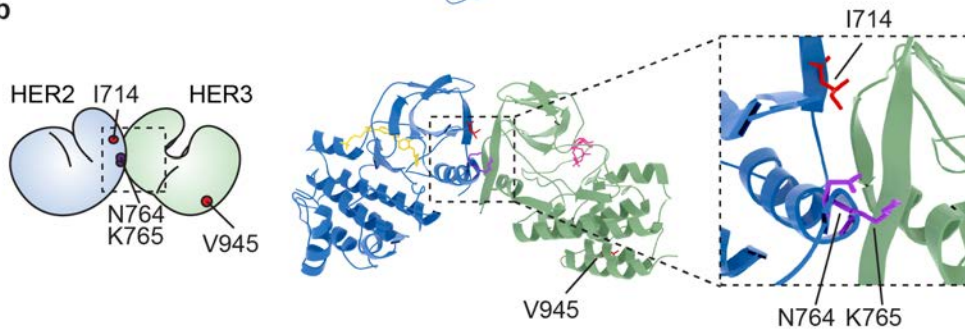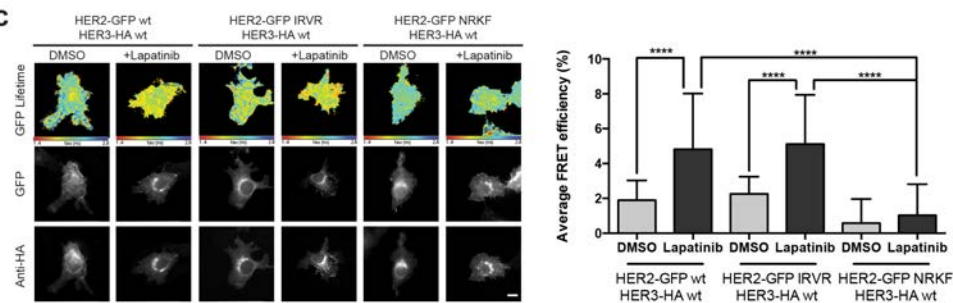542   Kuriyan, 2009b) (Figure 5b).

543

544

Figure 5

Figure 5 The lapatinib-induced HER2-HER3 dimer is in a symmetric orientation

(a) Lapatinib-bound HER2 (blue, lapatinib in yellow) and ATP analogue-bound HER3 (green, AMP-PNP in pink) were modelled in an EGFR-like symmetric dimer orientation (Jura, Endres, Engel, Deindl, Das, Lamers, et al., 2009a). Insert highlights the interaction interface. The schematic representation shows active dimer interface residues HER2^{I714} and HER3^{V945}, as well as the two residues in HER2 unique to this interface for further mutational analysis. **(b)** Lapatinib-bound HER2 in the HER3-like head-to-head symmetric dimer orientation (Jura, Shan, Cao, Shaw, & Kuriyan, 2009b). Dimer-specific residues are highlighted in the schematic. **(c)** MCF7 cells were transfected with vectors encoding HER2^{wt}-GFP, HER2$^{N764R/K765F}$-GFP or HER2$^{I748R/V750R}$-GFP and HER3^{wt}-HA. Cells were incubated for 24 hours, and inhibited with 10µM lapatinib for 1 hour, prior to fixation and staining with anti-HA antibody conjugated to Alexa-546. Data represented as mean ± SEM. ****, p≤0.0001, as analysed by one-way ANOVA. Scale bars 5 µm

Corresponding data and statistics available as Figure 5 – Source Data 1. Molecular model for the interactions in **(a)** and **(b)** available as Figure 5 – Source Data 2 and 3. Residues marking the dimer interface of the lapatinib-induced HER2-HER3 heterodimer, in either the EGFR-like

560   or HER3-like modelled conformations, including the per-residue solvent accessible surface area (in Å2), are

561   available as Figure 5 – Source Data 4.

562

563

564

565   **Figure 5-video 1**

566   Interface view of the molecular model of a lapatinib-induced HER2-HER3 heterodimer in the EGFR-like

567   conformation, with HER2^{I714} and HER3^{V945} highlighted, as well as model-specific interface residues HER2$^{I748/V750}$.

568   **Figure 5-video 2**

569   Interface highlight of the molecular model of a lapatinib-induced HER2-HER3 heterodimer in the HER3-like

570   conformation, with HER2^{I714} and HER3^{V945} highlighted, as well as model-specific interface residues

571   HER2$^{N764/K765}$.

572

Figure 5-figure supplement 1

a
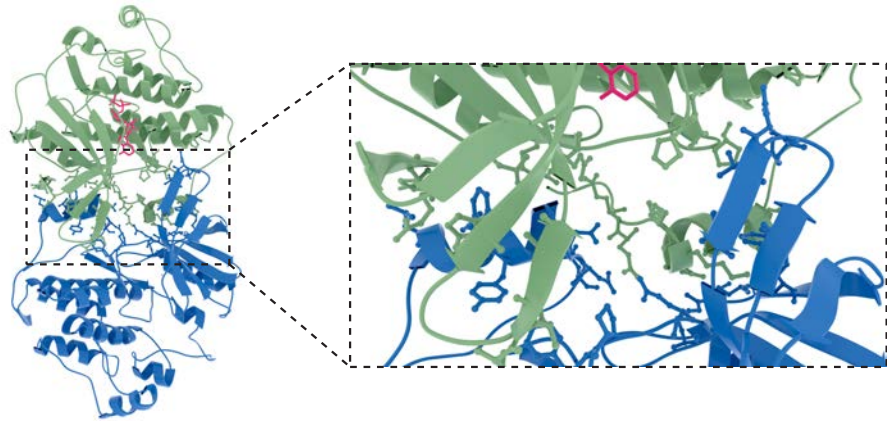
b

573

574 **Figure 5-figure supplement 1. Molecular models of potential orientations of the lapatinib-induced HER2-**

575 **HER3 dimer** Molecular model of the lapatinib-induced HER2-HER3 dimer in the **(a)** EGFR-like and **(b)** HER3-like

576 orientation with interface residues shown as sticks.

577

578

579

Head-to-head HER2-HER3 dimerisation is required for inhibitor-induced proliferation

580

581   Having presented modelling and FRET/FLIM data consistent with an orientation of the

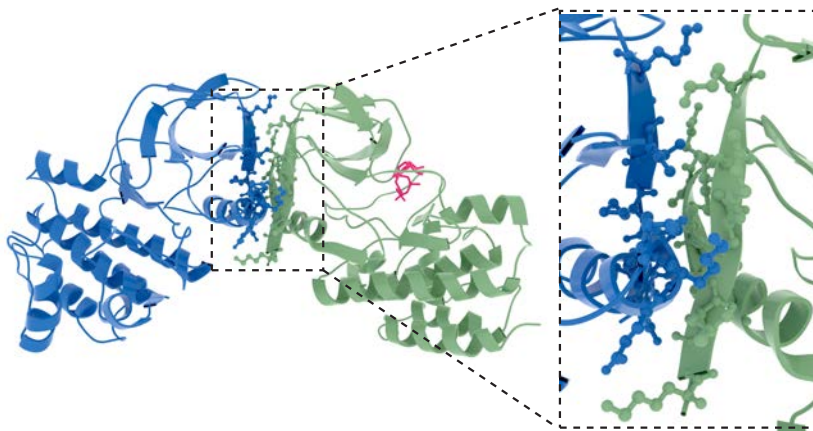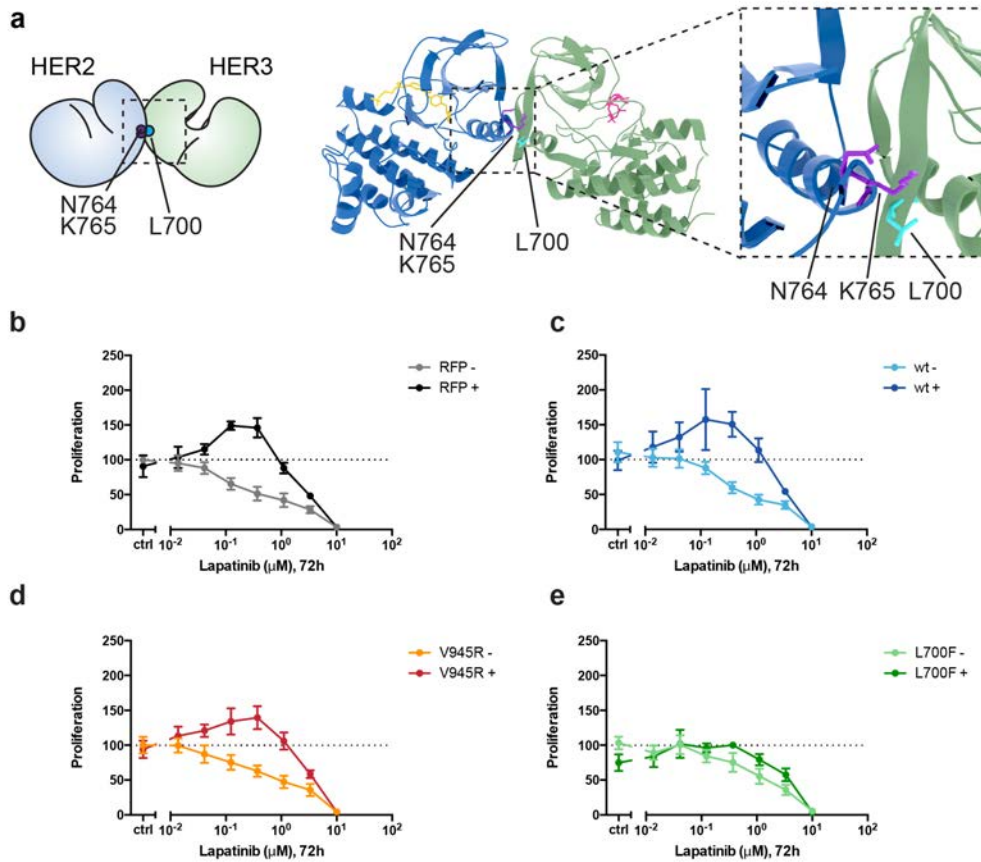582   lapatinib-induced HER2-HER3 dimer being distinct from the active activator/receiver dimer

583   interface, we sought to identify which type of HER2-HER3 interaction caused the NRG-

584   lapatinib co-stimulatory growth observed in 2D proliferation assays.

585   In these assays, we did not ectopically introduce the HER2$^{N764R/K765F}$ mutant because,

586   firstly, it might also disrupt the active, asymmetrical HER2-HER3 heterodimer interface and

587   secondly, SKBR3 cells have vast numbers of endogenous HER2 receptors that would hinder

588   analysis of the behaviour of ectopically expressed HER2$^{N764R/K765F}$. Instead we identified

589   HER3^{L700F} as the reciprocal mutant to HER2$^{N764R/K765F}$ (Figure 6a, Figure 6-video 1). We

590   introduced HER3^{L700F} into SKBR3 cells to investigate the role of the head-to-head, symmetric

591   dimer interface in the lapatinib-NRG synergistic proliferation described above. While the

592   HER3^{V945R} active dimer mutant did not disrupt drug-growth factor cooperative proliferation,

593   the HER3^{L700F} mutant did (Figure 6d-e). Both HER3^{L700F} and HER3^{V945R} were expressed on the

594   cell surface, as measured by flow cytometry (Figure 2-figure supplement 2). Combined, this

595   indicates that the inhibitor-induced heterodimer of HER2 and HER3 is consistent with a

596   head-to-head, symmetrical conformation, and it plays an important role in the synergistic

597   proliferative effects of lapatinib and NRG. Although this conformation has been described

598   from the HER3 kinase domain crystal lattice (Jura, Shan, Cao, Shaw, & Kuriyan, 2009b),

599   to our knowledge it is the first time a functional role has been ascribed to heterodimers

600   consistent with this interface in cells.

601

602

Figure 6

Figure 6. Disruption of the lapatinib-induced dimer inhibits lapatinib-NRG synergistic growth

(a) Molecular model of the lapatinib-induced HER2-HER3 dimer with the lapatinib-dimer interface residues HER2^{N764} and HER2^{K765} highlighted (purple), and a potential reciprocal residue HER3^{L700F} (cyan). **(b-e)** 2D proliferation assays of SKBR3 cells transfected with **(b)** RFP empty vector, **(c)** HER3^{wt}, **(d)** HER3^{V945R}, or **(e)** HER3^{L700F} and treated with lapatinib ± 10 nM NRG as before. Data represents mean ± SEM for six independent experiments, each performed in triplicate.

Corresponding data and statistics available as Figure 6 – Source Data 1

Figure 6-video 1

Interface highlight of the molecular model of a lapatinib-induced HER2-HER3 heterodimer in the HER3-like conformation, with HER2^{I714} and HER3^{V945} highlighted, as well as model-specific interface residues HER2$^{N764/K765}$ and HER3^{L700}.

Discussion

The conformational dynamics of HER2-HER3 heterodimerisation are an important consideration for evaluating existing and future targeted therapy intervention strategies against HER2$^+$ breast cancer and other HER family driven cancers. Here we show that the HER2 inhibitor lapatinib is paradoxically able to promote proliferative behaviour in HER2$^+$ breast cancer cells when administered in the presence of the HER3 ligand NRG. The synergy between growth factor and inhibitor requires an intricate, multi-step cascade of conformational events.

Lapatinib itself is able to promote heterodimerisation between the kinase domains of HER2 and HER3, stabilising an orientation consistent with a symmetric, head-to-head kinase domain heterodimer that is distinct from the canonical, asymmetric, head-to-tail active kinase domain orientation that occurs throughout the EGFR family. An analogous interface has previously been observed in the HER3 kinase domain crystal lattice (Jura, Shan, Cao, Shaw, & Kuriyan, 2009b); here we have provided modelling and cellular evidence of a heterodimer with an interface consistent to the one observed in the HER3 kinase domain crystal lattice. Sequestering HER2 and HER3 in these inactive, lapatinib-bound heterodimers was of benefit to NRG-mediated proliferative signalling. Our results, in which inhibitor binding drives dimer formation that boosts signalling and proliferation, shows some parallels with the inhibitor-induced signalling phenotypes in the RAF-family (Eyers et al., 1998; Hatzivassiliou et al., 2010; Mckay et al., 2011; Poulikakos et al., 2010; Thevakumaran et al., 2014)

While the FRET-FLIM analysis of the lapatinib-induced dimerisation was not able to differentiate between heterodimers or higher order oligomers, our clustering data shows that lapatinib is likely to induce higher order oligomers. Because of the modelled symmetrical nature of these lapatinib-induced dimers, in which both lapatinib-bound HER2 and HER3 would be conformationally available as 'activator' receptors for additional oligomerization partners, it is not inconceivable they may act as nucleation points for larger oligomeric signalling platforms. Such signalling arrays, in which mutual cooperativity increases signaling output, have been proposed for EGFR oligomers (Y. Huang et al., 2016).

650   The addition of ligand potentially causes rearrangements within these platforms through

651   the ligand-induced conformational ballet of multi-level interactions between the various

652   extracellular and intracellular domains of EGFR family receptors (reviewed in (Lemmon,

653   Schlessinger, & Ferguson, 2014)). The formation of lapatinib-induced oligomeric platforms

654   may facilitate a transition into active signalling heterodimers upon ligand binding, due to the

655   availability of dimerisation partners in immediate proximity within these drug-induced

656   oligomer platforms.

657

658   Both the lapatinib-induced HER2-HER3 heterodimerisation and the downstream lapatinib-

659   NRG synergistic effects on proliferation depended on the ability of HER3 to bind ATP.

660   Although usually classified as a pseudokinase, HER3 has been shown to retain a measure of

661   autophosphorylation activity (not transphosphorylation) under specific circumstances (Shi

662   et al., 2010). We show HER2-HER3 heterodimerisation and downstream proliferative

663   effects can be elicited by the addition of the HER3-binding inhibitor bosutinib, indicating

664   that nucleotide binding pocket occupation performs a structural role that is critical to HER3

665   function, and apparently independent of any retained catalytic activity. Observing increased

666   heterointeractions and cellular proliferation due to inhibition of an activity-deficient kinase

667   is a strong indication of the importance of ATP-binding in pseudokinases, and the necessity

668   of pocket-occupied structural conformers in sustaining protein-protein interactions and

669   subsequent downstream signalling output.

670

671   Because of the importance of HER3 in HER2-targeted therapy resistance, its conserved ATP

672   binding raised the possibility of targeting HER3 with ATP-competitive kinase inhibitors. Our

673   data shows, however, that stabilisation of the HER3 kinase domain with an ATP-competitive

674   kinase inhibitor can have a stimulating effect on HER2^{+} breast cancer cell proliferation. This

675   indicates that the development of small molecule targeted therapy against HER3 for use in

676   HER2^{+} breast cancer needs to be directed away from stabilising the HER3 ATP binding

677   pocket occupied conformer and rather towards stabilising the apo, inactive conformer. An

678   exception to this might be the development of irreversible, adamantane-linked inhibitors of

679   HER3 that target the receptor for proteosomal degradation (Xie et al., 2014).

680

681 The substantial effect that lower doses of lapatinib have on proliferation in the presence of

682 growth factor may have an impact on the establishment of lapatinib-resistance *in vivo*. This

683 is in accordance with the observation from xenograft models that resistance occurs much

684 more readily if lapatinib is administered continuously at low doses than if it's used

685 intermittently at high dose (Amin et al., 2010). Increased production of growth factors

686 (including NRG) is a well-described resistance mechanism against HER2-targeted therapy

687 (reviewed in(Claus et al., 2014)). NRG production by the microenvironment has also been

688 shown to play a role in metastatic spread of ovarian cancer cells that express high levels of

689 HER3 (Pradeep et al., 2014). High expression levels of NRG in HER2$^+$ breast cancer patients

690 showed a strong correlation with disease recurrence (Xia et al., 2013). Several somatic

691 mutations in HER3 observed in cancer fall within the extracellular domain and have a

692 potential effect on ligand binding affinity (Jaiswal et al., 2013). These mutations may

693 exacerbate the inhibitor-growth factor synergistic behaviour reported here.

694

695 Our results provide a potential molecular mechanism for the disappointing results observed

696 in a recent Phase III study of lapatinib used in an adjuvant setting (ALTTO trial) (Piccart-

697 Gebhart et al., 2016). The lapatinib-only arm of this study was terminated prematurely,

698 and the effects observed in the adjuvant setting for both lapatinib-trastuzumab co-

699 treatment and trastuzumab treatment followed by lapatinib were not significant. These

700 clinical results indicate there are complicating factors in hindering lapatinib efficacy in

701 patients, which may involve the expression levels of HER3 and NRG stimulation by a

702 complex tumour microenvironment. The complex relationships between distinct protein

703 conformation dynamics, formation of oligomeric assemblies, the availability of ligand, and

704 the various effects on downstream signalling need to all be part of the consideration when

705 applying targeted therapy to avoid potentially unexpected enhanced cancer cell

706 proliferation after inhibitor treatment.

707

708 **Materials and methods**

709

710 *Reagents and antibodies*

711 NRG1 was purchased from PeproTech. Lapatinib was a kind gift from Professor György Kéri

712 (Vichem Chemie Research Ltd Hungary). Bosutinib was purchased from LC Labs. Total HER2,

713   HER3, PKB, HER2 pY877, HER3 pY1289, PKB pS473 and ERK1/2 pT202/pY204 antibodies

714   were purchased from Cell Signaling Technology, anti-α-tubulin from Sigma, total ERK1/2

715   from Merck, and Alexa Fluor-488 conjugated anti-HER3 antibody from R&D systems.

716

717   *Cell culture and plasmid transfection*

718   MCF7 and ZR75 cells were cultured in DMEM supplemented with 10% FCS, SKBR3 cells were

719   grown in McCoys medium supplemented with 10% FCS. BT474, AU565, HCC1419, and

720   HCC1569 cells were grown in RPMI with 10% FCS. For BT474 cells 10 μg/ml bovine insulin

721   was included in the culture medium.

722   Cells were transfected with plasmid DNA using FuGene6 or FugeneHD (Roche), or

723   Lipofectamine LTX (Thermo Fisher Scientific) according to the manufacturer's protocol.

724   All cell lines were sourced from the Francis Crick Institute's Cell Services facility, where they

725   were tested negative for mycoplasma and authenticated via STR profiling.

726

727   *Proliferation assays*

728   For 2D proliferation assays, cells were plated at 1×10^4 cells/well in a 96-well plate. The

729   following day they were subjected to treatment for 72 hours, followed by addition of

730   CellTiter-Glo® reagent (Promega) and measured on an EnVision plate reader (Perkin Elmer).

731   CellTiter-Glo® data was normalised to the growth factor-null/inhibitor-null untreated

732   control. This caused some growth factor-treated plots to start at above-baseline levels,

733   which is an indication of the proliferative effect that growth factor treatment had in these

734   cells.

735   For 3D spheroid assays, 3×10^3 cells were plated in a 96-well, round-bottom, ultra-low

736   attachment plate (Corning) in the presence of 1% Matrigel (Corning). After three days of

737   growth, an equal volume of 2x media containing treatment conditions was added and

738   refreshed every three days for a total of eight days of treatment. Phase contrast images

739   were taken using a Zeiss Axiovert 40 CFL microscope with a Zeiss 5x A-plan objective and

740   analysed using ImageJ.

741

742   *Flow cytometry*

743   SKBR3 cells were transfected with RFP-HER3 mutants for 48 hours. Cells were pre-treated

744   with 0.5mM EDTA to facilitate removal from the substrate and stained for HER3

745   extracellular expression using Alexa Fluor-488 conjugated anti-HER3 antibody (R&D systems,

746   clone 66223) as per manufacturer's instructions. Briefly, cells were blocked using mouse

747   IgG (Santa Cruz Antibodies) for 15 minutes at room temperature, followed by incubation

748   with conjugated antibody for 30 minutes at room temperature in the dark. Cells were

749   washed in PBS, 0.5% BSA, 0.1% sodium azide three times before flow cytometric analysis

750   using a BD Fortessa instrument (BD). Results were analysed using the Flo-Jo software.

751

752   *FRET determination by FLIM measurements*

753   Fluorescence resonance energy transfer (FRET) is used to quantitate direct protein-protein

754   interactions and post-translational modifications. Processing of cells for FRET determination

755   by FLIM has been previously described (Barber et al., 2009; Parsons & Ng, 2002). FLIM

756   was performed using time-correlated single-photon counting (TCSPC) with a multiphoton

757   microscope system as described previously (Peter et al., 2005). For experiments

758   measuring endogenous protein, FRET pairs were Cy5-conjugated anti-HER2 IgG, and

759   Alexa546-conjugated anti-HER3 IgG. For exogenous protein measurements, FRET pairs were

760   HER2-GFP and HER3-HA with an anti-HA IgG, tagged with a Cy3 fluorophore. FRET efficiency

761   between the donor and acceptor bound proteins was calculated with the following equation

762   in each pixel and averaged per cell: FRET eff=1-tau(DA)/tau(control) where tau(DA) is the

763   lifetime displayed by cells co-expressing the donor and acceptor, whereas tau (control) is

764   the mean donor (GFP) lifetime, measured in the absence of the acceptor.

765

766   *Modelling HER2-HER3 dimers*

767   We modelled the HER2-HER3 dimer by comparative homology modelling using a multiple

768   templates approach. The active, asymmetric HER2-HER3 dimer was modelled using the

769   crystal structure of the active EGFR kinase domain (PDB ID 2GS2)(X. Zhang et al., 2006)

770   and one chain of the crystal structure of the HER3 homodimer (PDB ID 3KEX)(Jura, Shan,

771   Cao, Shaw, & Kuriyan, 2009b) as templates. To build the EGFR-like, inactive, symmetric

772   dimer we have used the crystal structure of the EGFR homodimer (PDB ID 3GT8)(Jura,

773   Endres, Engel, Deindl, Das, Lamers, et al., 2009a), the crystal structure of EGFR

774   complexed with lapatinib (PDB ID 1XKK)(Wood et al., 2004) and only one chain of the

775   crystal structure of the HER3 homodimer (PDB ID 3KEX)(Jura, Shan, Cao, Shaw, &

776   Kuriyan, 2009b). To build the HER3-like dimer we have used the HER3 homodimer

777   structure (PDB ID 3KEX)(Jura, Shan, Cao, Shaw, & Kuriyan, 2009b), the crystal structure

778   of EGFR lapatinib-bound (PDB ID 1XKK)(Wood et al., 2004) and the crystal structure of the

779   inactive EGFR AMP-PNP bound (PDB ID 2GS7)(X. Zhang et al., 2006). The sequence

780   alignment used to build the model has been created by using PRALINE with the homology-

781   extended alignment strategy (Simossis, 2005). We generated 200 three-dimensional

782   models using the MODELLER package(Sali & Blundell, 1993). The selected models were

783   chosen on the basis of the MODELLER objective function's DOPE score.

784   The volume of the HER2 ATP binding pocket was calculated with the SURFNET 1.5

785   package(Laskowski, 1995), where the cavity regions in a protein are built up by fitting a

786   probe sphere of 1.4 $Å^3$ into the spaces between atoms.

787   The structural alignment was performed using the multi-seq tool of the VMD 1.9.1

788   package(Humphrey, Dalke, & Schulten, 1996), and measurement of interaction surface

789   buried residues was performed using POPScomp(Kleinjung & Fraternali, 2005).

790

791   *Receptor clustering assays*

792   SKBR3 cells were treated with either 14nM Lapatinib or 41nM Bosutinib. HER2 and HER3

793   Affibody ligands were used to label the non-activated states of the receptors (HER2 from

794   Affibody Inc. and plasmid encoding the HER3 affibody was a gift from John Löfblom, protein

795   made in house and shown to bind specifically to HER3 receptors) and NRG-β1 (Peprotech)

796   was used to stimulate the cells. The conjugation of dyes (Invitrogen) to HER2 and HER3

797   ligands was done in house and the ratio of dye:ligand was confirmed to be ~1:1. The NRG-

798   dye conjugate has been shown to be as active as the unlabelled protein. We incubated cells

799   in 100nM HER2Affibody-Alexa488 + 50nM HER3Affibody-Alexa647 or 100nM HER2Affibody-

800   Alexa488 + 10nM NRG-Alexa647 ± drug for 1 hour. Cells were chemically fixed using 4%

801   paraformaldehyde (EMS solutions) + 0.5% glutaraldehyde (Sigma-Aldrich) diluted into ice-

802   cold PBS.

803   Samples were imaged using a Zeiss Elyra super-resolution microscope to stochastically

804   excite the Alexa488 and Alexa647 fluorophores bound to the receptors in the cells and to

805   image single molecules. Imaging was done in TIRF mode using a 100x oil immersion

806   objective lens. We used a 405nm laser line to aid fluorophore blinking and 488nm or 640nm

807   laser lines to excite the fluorophores, alternating the lasers to image the two receptors

808   independently every 300 frames, over a total of ~10,000 frames. The exposure time was

809   20ms. A minimum of two replicates of each sample were imaged generating at least 12

810   regions (25.6μm x 25.6μm) covering at least one cell per region. The Zen software localised

811   the single molecule spots in the cells, a threshold was set to discard background spots and

812   the co-ordinates of the positive localisations (typically 30,000+ for HER2 and 5,000+ for

813   HER3 per region) were passed into the Bayesian cluster identification algorithm (Rubin-

814   Delanchy et al., 2015)

815

816   The clustering algorithm expects the background and clusters to be uniformly distributed

817   over a rectangular ROI (Rubin-Delanchy et al., 2015). The analysed images mainly showed

818   single cells. Of interest are the HER2 and HER3 receptors in the cell membrane, which were

819   visible as a circular shape. In order to conform with the prerequisites of the clustering

820   algorithms, rectangular regions have been manually selected that tightly cover the cell

821   membrane using the most suitable angles (assessed by visual inspection). The whole cell

822   membrane has been covered in this way. The data selected by these regions has been

823   rotated so that the sides of the rectangles became parallel to the coordinate axis. The result

824   was used as input for the clustering algorithm and the algorithm was applied as described

825   by the protocol. The complete lists of molecules per cluster that have been produced by the

826   algorithm were used for the presentation.

827

828   *Recombinant HER3 KD purification*

829   The baculoviral HER3 kinase domain construct was kindly provided by Prof. Mark Lemmon,

830   University of Pennsylvania. Sf21 cells at $1x10^6$ cells/ml were infected with P3 virus ($7x10^7$

831   pfu/ml) at an MOI of 1.0 and allowed to grow for three days. The cells were lysed in lysis

832   buffer containing protease inhibitors, 1 mM DTT and 2 mM BME. The lysate was clarified by

833   centrifugation and incubated with NiNTA resin (Qiagen) for 30 mins at 4°C, after which the

834   resin was washed extensively with buffer containing 50 mM Hepes (pH 7.6), 300 mM NaCl, 2

835   mM BME, 5% glycerol, 10 mM imidazole. HER3 was eluted in the same buffer with 200 mM

836   imidazole added.

837   Each elution was centrifuged at 10,000 rpm to remove any precipitate or resin and applied

838   to a S200 gel filtration column in 50 mM HEPES (pH 7.6), 300 mM NaCl, 2 mM BME, 2.5%

839   glycerol.

840

Thermal Shift Assay (TSA)

841 Thermal shift assays were carried out as described in (Niesen, Berglund, & Vedadi,

842

843 2007). Briefly, in a 96-well RT-PCR plate (Life Technologies) 1 μg HER3 kinase domain/well

844 was incubated with 1 μM inhibitor or 200 μM ATP/10 mM $MgCl_2$ (as indicated) for 30 mins

845 at 4°C in the presence of Sypro Orange dye (Sigma). HER2 TSA experiments were performed

846 in a 384-well RT-PCR plate (Thermo Fisher Scientific). 0.5 μg of HER2 kinase domain/well

847 was incubated with 1μM lapatinib, 1μM bosutinib, or 200 μM ATP/10 mM $MgCl_2$ for 20 mins

848 at 4°C . HER3 measurements were taken on an Applied Biosystems 7500 Fast Real-Time PCR

849 machine, and HER2 measurements on an Applied Biosystems Quant Studio 7 PCR machine.

850 Data was trimmed and a Boltzmann sigmoidal curve fitted in GraphPad Prism 6. The

851 inflection point of the Boltzmann sigmoidal was taken as the T_m. Thermal shift ΔT_m values

852 were obtained by subtracting the T_m value of the kinase domain alone control.

853

854 *Western blot analysis*

855 Cells were plated at 0.5×10^5 cells/well in 24-well plates. Cells were lysed in 1x sample buffer

856 (containing 1 mM DTT), sonicated and centrifuged. After centrifugation, the lysates were

857 subjected to SDS-PAGE and analyzed by Western blotting.

858

859 *Cellular Thermal Shift Assay (CETSA)*

860 CETSA was performed with COS7 cells transfected with HER3[wt]-RFP, HER3[T787M]-RFP or

861 HER3[KGG]-RFP plasmids as described in (Jafari et al., 2014; Reinhard et al., 2015). Briefly, COS7

862 were treated with DMSO or 50nM bosutinib for 1h at 37°C. Cells were washed with PBS,

863 detached and washed again twice with cold PBS. Cell pellets were resuspended in cold PBS

864 with protease inhibitors (Roche) and 100μl of each cell suspension was transferred into

865 0.2ml PCR tubes. PCR tubes were heated for 3 min at 42°C or 50°C in a thermal cycler (DNA

866 Engine DYAD, MJ research, Peltier thermal cycler) and incubated at room temperature for

867 3min. Tubes were then immediately transferred onto ice, 35μl of cold PBS 1.4% NP-40 with

868 protease inhibitors were added and tubes were snap-frozen. Samples were then subjected

869 to two freeze-thaw (at 25 °C) cycles and cell lysates were centrifuged at 20,000g for 1h at

870 4 °C. Supernatants were carefully removed and analysed by Western blot.

871

Source data files

All source data is available as a ZIP file titled Claus_Patel_SOURCE-DATA_COMBINED, which

contains:

Figure 1 – Source Data 1 Numerical data and statistics relating to Figure 1

Figure 1 –figure supplement 1 - Source Data 1 Numerical data and statistics relating to

Figure 1-figure supplement 1

Figure 1 –figure supplement 2 - Source Data 1 Numerical data and statistics relating to

Figure 1-figure supplement 1

Figure 2 – Source Data 1 Numerical data and statistics relating to Figure 2

Figure 2 –figure supplement 1 - Source Data 1 Numerical data and statistics relating to

Figure 2-figure supplement 1

Figure 3 – Source Data 1 Numerical data and statistics relating to Figure 3

Figure 4 – Source Data 1 Numerical data and statistics relating to Figure 4

Figure 4 – Source Data 2 PDB structure file of molecular interaction model in Figure 4a

Figure 4 –figure supplement 1- Source Data 1 PDB structure file of inhibitor docking model

in Figure 4 **–figure supplement 1a**

Figure 4 –figure supplement 1- Source Data 2 PDB structure file of inhibitor docking model

in Figure **4 –figure supplement 1b**

Figure 5 – Source Data 1 Numerical data and statistics relating to Figure 5

Figure 5 – Source Data 2 PDB structure file of molecular interaction model in Figure 5a

Figure 5 – Source Data 3 PDB structure file of molecular interaction model in Figure 5b

Figure 5 – Source Data 4 Table with modelled interface residues, including the per-residue

solvent-accessible surface area in Å^2

Figure 6 – Source Data 1 Numerical data and statistics relating to Figure 6

911

References

913 Amin, D. N., Sergina, N. V., Ahuja, D., Mcmahon, M., Blair, J. A., Wang, D., et al.
914   (2010). Resiliency and Vulnerability in the HER2-HER3 Tumorigenic Driver.
915   *Science Translational Medicine*, *2*(16), 16ra7.
916   http://doi.org/10.1126/scitranslmed.3000389
917 Arteaga, C. L., Ramsey, T. T., Shawver, L. K., & Guyer, C. A. (1997). Unliganded
918   Epidermal Growth Factor Receptor Dimerization Induced by Direct Interaction of
919   Quinazolines with the ATP Binding Site. *The Journal of Biological Chemistry*,
920   *272*(37), 23247–23254. http://doi.org/10.1074/jbc.272.37.23247
921 Barber, P. R., Ameer-Beg, S. M., Gilbey, J., Carlin, L. M., Keppler, M., Ng, T. C., &
922   Vojnovic, B. (2009). Multiphoton time-domain fluorescence lifetime imaging
923   microscopy: practical application to protein-protein interactions using global
924   analysis. *Journal of the Royal Society Interface*, *6*(Suppl_1), S93–S105.
925   http://doi.org/10.1016/S0962-8924(01)01982-1
926 Baselga, J. J. B., & Swain, S. M. (2009). Novel anticancer targets: revisiting ERBB2
927   and discovering ERBB3. *Nature Rev Cancer*, *9*(7), 463–475.
928   http://doi.org/10.1038/nrc2656
929 Blackwell, K. L., Burstein, H. J., Storniolo, A. M., Rugo, H., Sledge, G., Koehler, M.,
930   et al. (2010). Randomized Study of Lapatinib Alone or in Combination With
931   Trastuzumab in Women With ErbB2-Positive, Trastuzumab-Refractory
932   Metastatic Breast Cancer. *Journal of Clinical Oncology : Official Journal of the
933   American Society of Clinical Oncology*, *28*(7), 1124–1130.
934   http://doi.org/10.1200/JCO.2008.21.4437
935 Boudeau, J., Miranda-Saavedra, D., Barton, G. J., & Alessi, D. R. (2006). Emerging
936   roles of pseudokinases. *Trends Cell Biol*, *16*(9), 443–452.
937   http://doi.org/10.1016/j.tcb.2006.07.003
938 Boxer, S. G., & Levinson, N. M. (2013). a conserved water-mediated hydrogen bond
939   network defines bosutinib's kinase selectivity. *Nature Chemical Biology*, *10*(2),
940   127–132. http://doi.org/10.1038/nchembio.1404
941 Bublil, E. M., Pines, G., Patel, G., Fruhwirth, G., Ng, T., & Yarden, Y. (2010). Kinase-
942   mediated quasi-dimers of EGFR. *The FASEB Journal : Official Publication of the
943   Federation of American Societies for Experimental Biology*.
944   http://doi.org/10.1096/fj.10-166199
945 Cameron, A. J. M., Escribano, C., Saurin, A. T., Kostelecky, B., & Parker, P. J.
946   (2009). PKC maturation is promoted by nucleotide pocket occupation

947   independently of intrinsic kinase activity. *Nature Structural & Molecular Biology*,
948   *16*(6), 624–630. http://doi.org/10.1038/nsmb.1606
949 Cameron, D., Piccart-Gebhart, M. J., Gelber, R. D., Procter, M., Goldhirsch, A., De
950   Azambuja, E., et al. (2017). 11 years' follow-up of trastuzumab after adjuvant
951   chemotherapy in HER2-positive early breast cancer: final analysis of the
952   HERceptin Adjuvant (HERA) trial. *Lancet*, *389*(10075), 1195–1205.
953   http://doi.org/10.1016/S0140-6736(16)32616-2
954 Claus, J., Cameron, A. J. M., & Parker, P. J. (2013). Pseudokinase drug intervention:
955   a potentially poisoned chalice. *Biochemical Society Transactions*, *41*(4), 1083–
956   1088.
957 Claus, J., Patel, G., Ng, T., & Parker, P. J. (2014). A role for the pseudokinase HER3
958   in the acquired resistance against EGFR- and HER2-directed targeted therapy.
959   *Biochemical Society Transactions*, *42*(4), 831–836.
960   http://doi.org/10.1042/BST20130078
961 Clayton, A. H. A. (2005). Ligand-induced Dimer-Tetramer Transition during the
962   Activation of the Cell Surface Epidermal Growth Factor Receptor-A
963   Multidimensional Microscopy Analysis. *The Journal of Biological Chemistry*,
964   *280*(34), 30392–30399. http://doi.org/10.1074/jbc.M504770200
965 Clayton, A. H. A., Tavarnesi, M. L., & Johns, T. G. (2007). Unligated Epidermal
966   Growth Factor Receptor Forms Higher Order Oligomers within Microclusters on
967   A431 Cells That Are Sensitive to Tyrosine Kinase Inhibitor Binding. *Biochemistry*,
968   *46*(15), 4589–4597. http://doi.org/10.1021/bi700002b
969 Coban, O., Zanetti-Dominguez, L. C., Matthews, D. R., Rolfe, D. J., Weitsman, G.,
970   Barber, P. R., et al. (2015). Effect of phosphorylation on EGFR dimer stability
971   probed by single-molecule dynamics and FRET/FLIM. *Biophysical Journal*,
972   *108*(5), 1013–1026. http://doi.org/10.1016/j.bpj.2015.01.005
973 Cui, J., Xiao, J., Tagliabracci, V. S., Wen, J., Rahdar, M., & Dixon, J. E. (2015). A
974   secretory kinase complex regulates extracellular protein phosphorylation. *eLife*,
975   *4*, e06120. http://doi.org/10.7554/eLife.06120
976 Cui, J., Zhu, Q., Zhang, H., Cianfrocco, M. A., Leschziner, A. E., Dixon, J. E., & Xiao,
977   J. (2017). Structure of Fam20A reveals a pseudokinase featuring a unique
978   disulfide pattern and inverted ATP-binding. *eLife*, *6*, 8.
979   http://doi.org/10.7554/eLife.23990
980 Davis, M. I., Hunt, J. P., Herrgard, S., Pietro Ciceri, Wodicka, L. M., Pallares, G., et
981   al. (2011). Comprehensive analysis of kinase inhibitor selectivity. *Nature
982   Biotechnology*, *29*(11), 1046–1051. http://doi.org/10.1038/nbt.1990
983 Dieras, V., Miles, D., Verma, S., Pegram, M., Welslau, M., Baselga, J. J. B., et al.
984   (2017). Trastuzumab emtansine versus capecitabine plus lapatinib in patients
985   with previously treated HER2-positive advanced breast cancer (EMILIA): a
986   descriptive analysis of final overall survival results from a randomised, open-
987   label, phase 3 trial. *The Lancet. Oncology*, *18*(6), 732–742.
988   http://doi.org/10.1016/S1470-2045(17)30312-1
989 Dong, C.-L., Guo, F.-C., & Xue, J. (2017). Computational insights into HER3
990   gatekeeper T768I resistance mutation to bosutinib in HER3-related breast
991   cancer. *Medicinal Chemistry Research*, 1–9. http://doi.org/10.1007/s00044-017-
992   1901-2
993 Eyers, P. A., Craxton, M., Morricel, N., Cohen, P., & Goedert, M. (1998). Conversion
994   of SB 203580-insensitive MAP kinase family members to drug-sensitive forms by

995 a single amino-acid substitution. *Chemistry & Biology*, *5*(6), 321–328.

996 Garrett, T. P. J., McKern, N. M., Lou, M., Elleman, T. C., Adams, T. E., Lovrecz, G.
997   O., et al. (2002). Crystal structure of a truncated epidermal growth factor receptor
998   extracellular domain bound to transforming growth factor alpha. *Cell*, *110*(6),
999   763–773.

1000 Geyer, C. E., Forster, J., Lindquist, D., Chan, S., Romieu, C. G., Pienkowski, T., et
1001   al. (2006). Lapatinib plus capecitabine for HER2-positive advanced breast
1002   cancer. *The New England Journal of Medicine*, *355*(26), 2733–2743.
1003   http://doi.org/10.1056/NEJMoa064320

1004 Hammarén, H. M., Ungureanu, D., Grisouard, J., Skoda, R. C., Hubbard, S. R., &
1005   Silvennoinen, O. (2015). ATP binding to the pseudokinase domain of JAK2 is
1006   critical for pathogenic activation. *Proceedings of the National Academy of*
1007   *Sciences of the United States of America*, *112*(15), 4642–4647.
1008   http://doi.org/10.1073/pnas.1423201112

1009 Hatzivassiliou, G., Song, K., Yen, I., Brandhuber, B. J., Anderson, D. J., Alvarado,
1010   R., et al. (2010). RAF inhibitors prime wild-type RAF to activate the MAPK
1011   pathway and enhance growth. *Nature*, *464*(7287), 431–435.
1012   http://doi.org/10.1038/nature08833

1013 Hildebrand, J. M., Tanzer, M. C., Lucet, I. S., Young, S. N., Spall, S. K., Sharma, P.,
1014   et al. (2014). Activation of the pseudokinase MLKL unleashes the four-helix
1015   bundle domain to induce membrane localization and necroptotic cell death.
1016   *Proceedings of the National Academy of Sciences of the United States of*
1017   *America*, *111*(42), 15072–15077. http://doi.org/10.1073/pnas.1408987111

1018 Huang, Y., Bharill, S., Karandur, D., Peterson, S. M., Marita, M., Shi, X., et al.
1019   (2016). Molecular basis for multimerization in the activation of the epidermal
1020   growth factor receptor. *eLife*, *5*, 18756. http://doi.org/10.7554/eLife.14107

1021 Humphrey, W., Dalke, A., & Schulten, K. (1996). VMD: visual molecular dynamics.
1022   *Journal of Molecular Graphics*, *14*(1), 33–8– 27–8.

1023 Huse, M., & Kuriyan, J. (2002). The conformational plasticity of protein kinases. *Cell*,
1024   *109*(3), 275–282.

1025 Jafari, R., Almqvist, H., Axelsson, H., Ignatushchenko, M., ck, T. L. A., Nordlund, P.
1026   A. R., & Molina, D. M. (2014). The cellular thermal shift assay for evaluating drug
1027   target interactions in cells. *Nature Protocols*, *9*(9), 2100–2122.
1028   http://doi.org/10.1038/nprot.2014.138

1029 Jaiswal, B. S., Kljavin, N. M., Stawiski, E. W., Chan, E., Parikh, C., Durinck, S., et al.
1030   (2013). Oncogenic ERBB3 mutations in human cancers. *Cancer Cell*, *23*(5),
1031   603–617. http://doi.org/10.1016/j.ccr.2013.04.012

1032 Jeffrey, P. D., Russo, A. A., Polyak, K., Gibbs, E., Hurwitz, J., Massagué, J., &
1033   Pavletich, N. P. (1995). Mechanism of CDK activation revealed by the structure
1034   of a cyclinA-CDK2 complex. *Nature*, *376*(6538), 313–320.
1035   http://doi.org/10.1038/376313a0

1036 Jura, N., Endres, N. F., Engel, K., Deindl, S., Das, R., Lamers, M. H., et al. (2009a).
1037   Mechanism for activation of the EGF receptor catalytic domain by the
1038   juxtamembrane segment. *Cell*, *137*(7), 1293–1307.
1039   http://doi.org/10.1016/j.cell.2009.04.025

1040 Jura, N., Shan, Y., Cao, X., Shaw, D. E., & Kuriyan, J. (2009b). Structural analysis of
1041   the catalytically inactive kinase domain of the human EGF receptor 3.
1042   *Proceedings of the National Academy of Sciences of the United States of*

America, *106*(51), 21608–21613. http://doi.org/10.1073/pnas.0912101106

Kleinjung, J., & Fraternali, F. (2005). POPSCOMP: an automated interaction analysis of biomolecular complexes. *Nucleic Acids Research*, *33*(Web Server), W342–W346. http://doi.org/10.1093/nar/gki369

Krop, I. E., Kim, S.-B., Martin, A. G., LoRusso, P. M., Ferrero, J.-M., Badovinac-Crnjevic, T., et al. (2017). Trastuzumab emtansine versus treatment of physician's choice in patients with previously treated HER2-positive metastatic breast cancer (TH3RESA): final overall survival results from a randomised open-label phase 3 trial. *The Lancet. Oncology*, *18*(6), 743–754. http://doi.org/10.1016/S1470-2045(17)30313-3

Laskowski, R. A. (1995). SURFNET: a program for visualizing molecular surfaces, cavities, and intermolecular interactions. *Journal of Molecular Graphics*, *13*(5), 323–30– 307–8.

Lemmon, M. A., Schlessinger, J., & Ferguson, K. M. (2014). The EGFR family: not so prototypical receptor tyrosine kinases. *Cold Spring Harbor Perspectives in Biology*, *6*(4), a020768–a020768. http://doi.org/10.1101/cshperspect.a020768

Lichtner, R. B., Menrad, A., Sommer, A., Klar, U., & Schneider, M. R. (2001). Signaling-inactive epidermal growth factor receptor/ligand complexes in intact carcinoma cells by quinazoline tyrosine kinase inhibitors. *Cancer Research*, *61*(15), 5790–5795.

Littlefield, P., Liu, L., Mysore, V., Shan, Y., Shaw, D. E., & Jura, N. (2014). Structural analysis of the EGFR/HER3 heterodimer reveals the molecular basis for activating HER3 mutations. *Science Signaling*, *7*(354), ra114–ra114. http://doi.org/10.1126/scisignal.2005786

Liu, P., Cleveland, T. E., Bouyain, S., Byrne, P. O., Longo, P. A., & Leahy, D. J. (2012). A single ligand is sufficient to activate EGFR dimers. *Proceedings of the National Academy of Sciences of the United States of America*, *109*(27), 10861–10866. http://doi.org/10.1073/pnas.1201114109

Lovekin, C., Ellis, I. O., Locker, A., Robertson, J. F., Bell, J., Nicholson, R., et al. (1991). c-erbB-2 oncoprotein expression in primary and advanced breast cancer. *British Journal of Cancer*, *63*(3), 439.

Mckay, M. M., Ritt, D. A., & Morrison, D. K. (2011). RAF Inhibitor-Induced KSR1/B-RAF Binding and Its Effects on ERK Cascade Signaling. *Current Biology*, *21*(7), 563–568. http://doi.org/10.1016/j.cub.2011.02.033

Mi, L.-Z., Lu, C., Li, Z., Nishida, N., Walz, T., & Springer, T. A. (2011). Simultaneous visualization of the extracellular and cytoplasmic domains of the epidermal growth factor receptor. *Nature Structural & Molecular Biology*, *18*(9), 984–989. http://doi.org/10.1038/nsmb.2092

Murphy, J. M., Czabotar, P. E., Hildebrand, J. M., Lucet, I. S., Zhang, J.-G., Alvarez-Diaz, S., et al. (2013). The pseudokinase MLKL mediates necroptosis via a molecular switch mechanism. *Immunity*, *39*(3), 443–453. http://doi.org/10.1016/j.immuni.2013.06.018

Murphy, J. M., Zhang, Q., Young, S. N., Reese, M. L., Bailey, F. P., Eyers, P. A., et al. (2014). A robust methodology to subclassify pseudokinases based on their nucleotide-binding properties. *The Biochemical Journal*, *457*(2), 323–334. http://doi.org/10.1042/BJ20131174

Nagy, P., Claus, J., Jovin, T. M., & Arndt-Jovin, D. J. (2010). Distribution of resting and ligand-bound ErbB1 and ErbB2 receptor tyrosine kinases in living cells using

number and brightness analysis. *Proceedings of the National Academy of Sciences of the United States of America*, *107*(38), 16524–16529. http://doi.org/10.1073/pnas.1002642107

Needham, S. R., Roberts, S. K., Arkhipov, A., Mysore, V. P., Tynan, C. J., Zanetti-Domingues, L. C., et al. (2016). EGFR oligomerization organizes kinase-active dimers into competent signalling platforms. *Nature Communications*, *7*, 13307. http://doi.org/10.1038/ncomms13307

Niesen, F. H., Berglund, H., & Vedadi, M. (2007). The use of differential scanning fluorimetry to detect ligand interactions that promote protein stability. *Nature Protocols*, *2*(9), 2212–2221. http://doi.org/10.1038/nprot.2007.321

Novotny, C. J., Pollari, S., Park, J. H., Lemmon, M. A., Shen, W., & Shokat, K. M. (2016). Overcoming resistance to HER2 inhibitors through state-specific kinase binding. *Nature Chemical Biology*, 1–10. http://doi.org/10.1038/nchembio.2171

Ogiso, H., Ishitani, R., Nureki, O., Fukai, S., Yamanaka, M., Kim, J.-H., et al. (2002). Crystal structure of the complex of human epidermal growth factor and receptor extracellular domains. *Cell*, *110*(6), 775–787.

Okuzumi, T., Fiedler, D., Zhang, C., Gray, D. C., Aizenstein, B., Hoffman, R., & Shokat, K. M. (2009). Inhibitor hijacking of Akt activation. *Nature Chemical Biology*, *5*(7), 484–493. http://doi.org/10.1038/nchembio.183

Ortiz-Zapater, E., Lee, R. W., Owen, W., Weitsman, G., Fruhwirth, G., Dunn, R. G., et al. (2017). MET-EGFR dimerization in lung adenocarcinoma is dependent on EGFR mtations and altered by MET kinase inhibition. *PLoS ONE*, *12*(1), e0170798–19. http://doi.org/10.1371/journal.pone.0170798

Owens, M. A., Horten, B. C., & Da Silva, M. M. (2011). HER2 Amplification Ratios by Fluorescence In Situ Hybridization and Correlation with Immunohistochemistry in a Cohort of6556 Breast Cancer Tissues. *Clinical Breast Cancer*, *5*(1), 63–69. http://doi.org/10.3816/CBC.2004.n.011

Papa, F. R., Zhang, C., Shokat, K. M., & Walter, P. (2003). Bypassing a kinase activity with an ATP-competitive drug. *Science (New York, NY)*, *302*(5650), 1533–1537. http://doi.org/10.1126/science.1090031

Parsons, M., & Ng, T. (2002). Intracellular coupling of adhesion receptors: molecular proximity measurements. *Methods in Cell Biology*, *69*, 261–278.

Peter, M., Ameer-Beg, S. M., Hughes, M. K. Y., Keppler, M. D., Prag, S., Marsh, M., et al. (2005). Multiphoton-FLIM Quantification of the EGFP-mRFP1 FRET Pair for Localization of Membrane Receptor-Kinase Interactions. *Biophysical Journal*, *88*(2), 1224–1237. http://doi.org/10.1529/biophysj.104.050153

Piccart-Gebhart, M., Holmes, E., Baselga, J. J. B., De Azambuja, E., Dueck, A. C., Viale, G., et al. (2016). Adjuvant Lapatinib and Trastuzumab for Early Human Epidermal Growth Factor Receptor 2-Positive Breast Cancer: Results From the Randomized Phase III Adjuvant Lapatinib and/or Trastuzumab Treatment Optimization Trial. *Journal of Clinical Oncology*, *34*(10), 1034–1042. http://doi.org/10.1200/JCO.2015.62.1797

Poulikakos, P. I., Zhang, C., Bollag, G., Shokat, K. M., & Rosen, N. (2010). RAF inhibitors transactivate RAF dimers and ERK signalling in cells with wild-type BRAF. *Nature*, *464*(7287), 427–430. http://doi.org/10.1038/nature08902

Pradeep, S., Kim, S. W., Wu, S. Y., Nishimura, M., Chaluvally-Raghavan, P., Miyake, T., et al. (2014). Hematogenous Metastasis of Ovarian Cancer: Rethinking Mode of Spread. *Cancer Cell*, *26*(1), 77–91.

1139   http://doi.org/10.1016/j.ccr.2014.05.002

1140 Reinhard, F. B. M., Eberhard, D., Werner, T., Franken, H., Childs, D., Doce, C., et al.
1141   (2015). Thermal proteome profiling monitors ligand interactions with cellular
1142   membrane proteins. *Nature Methods*, 1–6. http://doi.org/10.1038/nmeth.3652

1143 Ross, F. A., Hawley, S. A., Auciello, F. R., Gowans, G. J., Atrih, A., Lamont, D. J., &
1144   Hardie, D. G. (2017). Mechanisms of Paradoxical Activation of AMPK by the
1145   Kinase Inhibitors SU6656 and Sorafenib. *Cell Chemical Biology*, *24*(7), 813–
1146   824.e4. http://doi.org/10.1016/j.chembiol.2017.05.021

1147 Rubin-Delanchy, P., Burn, G. L., Griffié, J., Williamson, D. J., Heard, N. A., Cope, A.
1148   P., & Owen, D. M. (2015). Bayesian cluster identification in single-molecule
1149   localization microscopy data. *Nature Methods*, *12*(11), 1072–1076.
1150   http://doi.org/10.1038/nmeth.3612

1151 Saffarian, S., Li, Y., Elson, E. L., & Pike, L. J. (2008). Oligomerization of the EGF
1152   Receptor Investigated by Live Cell Fluorescence Intensity Distribution Analysis.
1153   *Biophysical Journal*, *93*(3), 1021–1031.
1154   http://doi.org/10.1529/biophysj.107.105494

1155 Sali, A., & Blundell, T. L. (1993). Comparative protein modelling by satisfaction of
1156   spatial restraints. *Journal of Molecular Biology*, *234*(3), 779–815.
1157   http://doi.org/10.1006/jmbi.1993.1626

1158 Scheeff, E. D., Eswaran, J., Bunkoczi, G., Knapp, S., & Manning, G. (2009).
1159   Structure of the pseudokinase VRK3 reveals a degraded catalytic site, a highly
1160   conserved kinase fold, and a putative regulatory binding site. *Structure*, *17*(1),
1161   128–138. http://doi.org/10.1016/j.str.2008.10.018

1162 Sergina, N. V., Rausch, M., Wang, D., Blair, J., Hann, B., Shokat, K. M., & Moasser,
1163   M. M. (2007). Escape from HER-family tyrosine kinase inhibitor therapy by the
1164   kinase-inactive HER3. *Nature*, *445*(7126), 437–441.
1165   http://doi.org/10.1038/nature05474

1166 Shi, F., Telesco, S. E., Liu, Y., Radhakrishnan, R., & Lemmon, M. A. (2010).
1167   ErbB3/HER3 intracellular domain is competent to bind ATP and catalyze
1168   autophosphorylation. *Proceedings of the National Academy of Sciences of the
1169   United States of America*, *107*(17), 7692–7697.
1170   http://doi.org/10.1073/pnas.1002753107

1171 Simossis, V. A. (2005). Homology-extended sequence alignment. *Nucleic Acids
1172   Research*, *33*(3), 816–824. http://doi.org/10.1093/nar/gki233

1173 Slamon, D. J., Clark, G. M., Wong, S. G., Levin, W. J., Ullrich, A., & McGuire, W. L.
1174   (1987). Human breast cancer: correlation of relapse and survival with
1175   amplification of the HER-2/neu oncogene. *Science (New York, NY)*, *235*(4785),
1176   177–182.

1177 Sliwkowski, M. X., Schaefer, G., Akita, R. W., Lofgren, J. A., Fitzpatrick, V. D.,
1178   Nuijens, A., et al. (1994). Coexpression of erbB2 and erbB3 proteins
1179   reconstitutes a high affinity receptor for heregulin. *The Journal of Biological
1180   Chemistry*, *269*(20), 14661–14665.

1181 Swain, S. M., Baselga, J. J. B., Kim, S.-B., Ro, J., Semiglazov, V., Campone, M., et
1182   al. (2015). Pertuzumab, trastuzumab, and docetaxel in HER2-positive metastatic
1183   breast cancer. *The New England Journal of Medicine*, *372*(8), 724–734.
1184   http://doi.org/10.1056/NEJMoa1413513

1185 Thevakumaran, N., Lavoie, H., Critton, D. A., Tebben, A., Marinier, A., Sicheri, F., &
1186   Therrien, M. (2014). Crystal structure of a BRAF kinase domain monomer

explains basis for allosteric regulation. *Nature Structural & Molecular Biology*, *22*(1), 37–43. http://doi.org/10.1038/nsmb.2924

Thiel, K. W., & Carpenter, G. (2007). Epidermal growth factor receptor juxtamembrane region regulates allosteric tyrosine kinase activation. *Proceedings of the National Academy of Sciences of the United States of America*, *104*(49), 19238–19243. http://doi.org/10.1073/pnas.0703854104

van Lengerich, B., Agnew, C., Puchner, E. M., Huang, B., & Jura, N. (2017). EGF and NRG induce phosphorylation of HER3/ERBB3 by EGFR using distinct oligomeric mechanisms. *Proceedings of the National Academy of Sciences of the United States of America*, *114*(14), E2836–E2845. http://doi.org/10.1073/pnas.1617994114

Verma, S., Miles, D., Gianni, L., Krop, I. E., Welslau, M., Baselga, J. J. B., et al. (2012). Trastuzumab emtansine for HER2-positive advanced breast cancer. *The New England Journal of Medicine*, *367*(19), 1783–1791. http://doi.org/10.1056/NEJMoa1209124

Wang, L., Perera, B. G. K., Hari, S. B., Bhhatarai, B., Backes, B. J., Seeliger, M. A., et al. (2012). Divergent allosteric control of the IRE1α endoribonuclease using kinase inhibitors. *Nature Chemical Biology*, *8*(12), 982–989. http://doi.org/10.1038/nchembio.1094

Wilson, T. R., Fridlyand, J., Yan, Y., Penuel, E., Burton, L., Chan, E., et al. (2012). Widespread potential for growth-factor-driven resistance to anticancer kinase inhibitors. *Nature*, *487*(7408), 505–509. http://doi.org/10.1038/nature11249

Wood, E. R., Truesdale, A. T., McDonald, O. B., Yuan, D., Hassell, A., Dickerson, S. H., et al. (2004). A unique structure for epidermal growth factor receptor bound to GW572016 (Lapatinib): relationships among protein conformation, inhibitor off-rate, and receptor activity in tumor cells. *Cancer Research*, *64*(18), 6652–6659. http://doi.org/10.1158/0008-5472.CAN-04-1168

Xia, W., Petricoin, E. F., Zhao, S., Liu, L., Osada, T., Cheng, Q., et al. (2013). An heregulin-EGFR-HER3 autocrine signaling axis can mediate acquired lapatinib resistance in HER2+ breast cancer models. *Breast Cancer Res*, *15*(5), R85. http://doi.org/10.1186/bcr3480

Xie, T., Lim, S. M., Westover, K. D., Dodge, M. E., Ercan, D., Ficarro, S. B., et al. (2014). Pharmacological targeting of the pseudokinase Her3. *Nature Chemical Biology*, *10*(12), 1006–1012. http://doi.org/10.1038/nchembio.1658

Yang, S., Raymond-Stintz, M. A., Ying, W., Zhang, J., Lidke, D. S., Steinberg, S. L., et al. (2007). Mapping ErbB receptors on breast cancer cell membranes during signal transduction. *Journal of Cell Science*, *120*(16), 2763–2773. http://doi.org/10.1242/jcs.007658

Yarden, Y., & Pines, G. (2012). The ERBB network: at last, cancer therapy meets systems biology. *Nature Rev Cancer*, *12*(8), 553–563. http://doi.org/10.1038/nrc3309

Zeqiraj, E., Filippi, B. M., Deak, M., Alessi, D. R., & van Aalten, D. M. V. (2009a). Structure of the LKB1-STRAD-MO25 complex reveals an allosteric mechanism of kinase activation. *Science (New York, NY)*, *326*(5960), 1707–1711. http://doi.org/10.1126/science.1178377

Zeqiraj, E., Filippi, B. M., Goldie, S., Navratilova, I., Boudeau, J., Deak, M., et al. (2009b). ATP and MO25α Regulate the Conformational State of the STRADα Pseudokinase and Activation of the LKB1 Tumour Suppressor. *PLoS Biology*,

1235   *7*(6), e1000126. http://doi.org/10.1371/journal.pbio.1000126.s009

1236   Zhang, R., Fruhwirth, G. O., Coban, O., Barrett, J. E., Burgoyne, T., Lee, S. H., et al.
1237   (2017). Probing the Heterogeneity of Protein Kinase Activation in Cells by Super-
1238   resolution Microscopy. *ACS Nano*, *11*(1), 249–257.
1239   http://doi.org/10.1021/acsnano.6b05356

1240   Zhang, X., Gureasko, J., Shen, K., Cole, P. A., & Kuriyan, J. (2006). An allosteric
1241   mechanism for activation of the kinase domain of epidermal growth factor
1242   receptor. *Cell*, *125*(6), 1137–1149. http://doi.org/10.1016/j.cell.2006.05.013

1243